Biomacromolecules

pubs.acs.org/Biomac

Article

Postmodification with Polycations Enhances Key Properties of Alginate-Based Multicomponent Microcapsules

Faeze Dorchei, Abolfazl Heydari, Zuzana Kroneková, Juraj Kronek, Michal Pelach, Zuzana Cseriová, Dušan Chorvát, Fernando Zúñiga-Navarrete, Peter D. Rios, James McGarrigle, Sofia Ghani, Douglas Isa, Ira Joshi, Kalaiyarasi Vasuthas, Anne Mari A. Rokstad, José Oberholzer, Vladimír Raus,* and Igor Lacík*

Cite This: *Biomacromolecules* 2024, 25, 4118–4138

Read Online

ACCESS | Metrics & More | Article Recommendations | Supporting Information

ABSTRACT: Postmodification of alginate-based microspheres with polyelectrolytes (PEs) is commonly used in the cell encapsulation field to control microsphere stability and permeability. However, little is known about how different applied PEs shape the microsphere morphology and properties, particularly *in vivo*. Here, we addressed this question using model multicomponent alginate-based microcapsules postmodified with PEs of different charge and structure. We found that the postmodification can enhance or impair the mechanical resistance and biocompatibility of microcapsules implanted into a mouse model, with polycations surprisingly providing the best results. Confocal Raman microscopy and confocal laser scanning microscopy (CLSM) analyses revealed stable interpolyelectrolyte complex layers within the parent microcapsule, hindering the access of higher molar weight PEs into the microcapsule core. All microcapsules showed negative surface zeta potential, indicating that the postmodification PEs get hidden within the microcapsule membrane, which agrees with CLSM data. Human whole blood assay revealed complex behavior of microcapsules regarding their inflammatory and coagulation potential. Importantly, most of the postmodification PEs, including polycations, were found to be benign toward the encapsulated model cells.

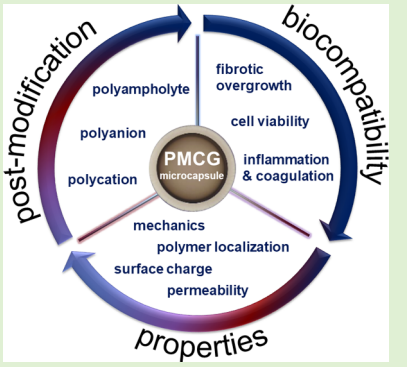

INTRODUCTION

Polyelectrolytes (PEs) are finding extensive applications in diverse fields, including environmental technologies, biotechnology, biomedicine, pharmacy, energy storage and conversion, and electronics.[1−7] PE-based materials often take the form of noncovalently cross-linked hydrogels that can be conveniently produced via processes such as ionotropic gelation or interpolyelectrolyte complexation under physiological conditions. Importantly, these materials often show the functional properties necessary for their applications *in vivo*. One prominent application involves the encapsulation of living cells in PE-based hydrogels, a strategy used in various cell therapies to prevent graft rejection while avoiding the side effects of systemic immunosuppression.[8] The encapsulated cells continuously secrete therapeutic molecules, such as hormones, with the hydrogel shielding the cells from the immune system and ensuring their long-term survival and function.[9]

Microencapsulation of insulin-producing cells in PE-based hydrogel microspheres is considered as a next-generation treatment for type I diabetes.[10] Although the principle of immunoisolated pancreatic islet transplantation was proposed more than four decades ago,[11] it still remains unavailable in clinical practice. Two contradictory requirements make this strategy particularly challenging: the free communication of the transplanted islets with the host organism (e.g., the nutrient access and insulin release) and the "invisibility" of the graft to the host immune system. Fulfilling these requirements is closely tied to the control of key microsphere properties, including biocompatibility, stability, and permeability.[12]

Among different materials used for the preparation of microspheres for pancreatic islet encapsulation, PE-based materials, and particularly those containing sodium alginate (SA) as the main component, have attracted the most attention.[9] SA has been applied to fabricate simple ionotropically cross-linked microspheres (so-called alginate microbeads)[13] as well as more complex variants involving additional PEs, embedded via interpolyelectrolyte complex (IPEC) formation, that are typically denoted as microcapsules.[14−17] Cell encapsulation in alginate microspheres has been the subject of several clinical trials; however, the expected clinical benefit is yet to be reached.[10] Current efforts in alginate microsphere development are primarily centered on enhancing the biomaterial biocompatibility through various approaches, including microbead size control,[18] introduction of antifibrotic

Received: February 18, 2024
Revised: May 31, 2024
Accepted: May 31, 2024
Published: June 10, 2024

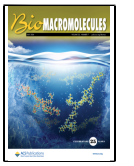

https://doi.org/10.1021/acs.biomac.4c00222
Biomacromolecules 2024, 25, 4118−4138

moieties onto the microbead surface,[19] transplantation site selection,[13] incorporation of antifibrotic chemokine CXCL12,[20] and the use of sulfated SA[21] or zwitterion-modified SA.[22] Nevertheless, the inherent drawbacks of alginate microbeads, e.g., the long-term structural instability[23,24] or insufficient molar weight cutoff (MWCO) control,[25] have not been fully addressed. Importantly, these problems can be potentially mitigated by introducing an additional interface into the microsphere through an IPEC formation. Interestingly, the pioneering report by Lim and Sun already proposed that the stability and permeability of alginate microbeads could be controlled by coating with poly(L-lysine) (PLL) and polyethyleneimine, utilizing the residual charges in the alginate hydrogel network.[11] Later, this approach was further developed, mainly by employing PLL and poly(L-ornithine) as additional PEs.[14,16,26] However, the potentially inflammatory character of polycations of the PLL type has been highlighted in a number of studies.[10,15,27−31] Consequently, polycation-containing microspheres tend to be considered as potentially problematic materials with high inflammation potential within the encapsulation community. Nevertheless, the situation is more complex because microsphere properties and performance may differ dramatically depending on the polycation structure and its localization within the microsphere hydrogel network. Indeed, some types of cation-containing alginate-based microspheres, e.g., polyallylamine-coated alginate microbeads[27] and, particularly, the so-called PMCG microcapsules,[17,32] consisting of polyanions SA and sodium cellulose sulfate, SCS, and the polycation poly(methylene-*co*-cyanoguanidine), PMCG, showed lower induction of inflammation (complement and inflammatory cytokines) in the human whole blood assay (WBA) as compared to PLL-coated alginate microbeads[29,30] and minimal pericapsular fibrotic overgrowth (PFO) in animal models.[33] Especially the multicomponent systems of the PMCG microcapsule type may thus represent an alternative design for which the interaction of different present PEs yet remains to be fully elucidated. More specifically, additional data are critically needed in order to assess the interactions of PE-based hydrogel microspheres with externally applied PEs and to recognize whether this strategy can improve the key microsphere properties (e.g., mechanical resistance, permeability control, or long-term stability *in vivo*) without significantly compromising their biocompatibility.

In this work, we synthesized a library of cationic, anionic, and ampholytic PEs and employed them to postmodify PMCG microcapsules as model PE-based microspheres. We took advantage of the PMCG microcapsule's unique multicomponent character whereby the unsaturated charges in the polyanionic (SA, SCS) and polycationic (PMCG) components can be used to form IPEC with the additionally applied PE. We then applied a battery of methods—an IgG permeability assay, inverse size-exclusion chromatography (iSEC), confocal Raman microscopy (CRM), confocal laser scanning microscopy (CLSM), zeta potential measurements, cell viability assay, and human WBA—to study how the postmodification impacts on the key microcapsule properties and to obtain further insights into the underlying phenomena. This was complemented by *in vivo* data, obtained using a mouse model, that unveiled the potential of the postmodification strategy in the context of cell therapies. Importantly, we revealed that certain polycations significantly enhanced the biocompatibility and *in vivo* mechanical stability of PMCG microcapsules, while keeping the postmodified microcapsules noncytotoxic to the encapsulated model cells and maintaining a similarly low level of inflammatory potential as the parent PMCG microcapsules.

EXPERIMENTAL SECTION

Materials. UltraPure sodium alginate (SA; Pronova UP MVM, lot # FP-501-04, 54 mol % mannuronic units) was obtained from NovaMatrix (Sandvika, Norway). The weight-average molar weight, M_w, for this SA lot (271 000 g·mol^{-1}, $Đ$ = 1.8) was determined in our laboratory by size-exclusion chromatography equipped with multi-angle laser-light scattering and refractive index detectors (SEC-MALS).[34] Chitosan 95/20 (M_w = 76 000 g·mol^{-1} and degree of acetylation DA = 2.5%, as determined in our laboratory[35]) was obtained from Heppe Medical Chitosan GmbH (Halle, Germany). Dextran (M_w ∼ 100 000−150 000 g·mol^{-1} as indicated by the manufacturer), 1,3-propane sultone (PrS, 98%), glycidyltrimethylammonium chloride (GTMAC, ≥90%, 20−25% water content), fluorescein 5(6)-isothiocyanate (≥90%, FITC), Whatman filter paper type 1450-917, SO_3·DMF complex (97%), sodium acetate (≥99%), 1-cyanoguanidine (99%), paraformaldehyde (95%), ammonium chloride (≥99.5%), sodium carbonate (≥99.5%), sodium bicarbonate (≥99.5%), Dulbecco's modified Eagle's medium (DMEM), RPMI, and CMRL-1066 media, human serum albumin (HSA), horse serum (HS), and fetal bovine serum (FBS) were obtained from Sigma Aldrich. Dialysis membrane (Spectra/Por, molar weight cutoff, MWCO, 1 000 and 3 500 g·mol^{-1}) was purchased from Spectrum Laboratories Inc. (New Brunswick, NJ). DMF (≥99.5%) was purchased from Fisher Chemical and stored under argon over 3 Å molecular sieves. An ELISA kit for the human terminal complement complex was obtained from Hycult Biotech, Uden, Netherlands. ELISA kit for mice cytokines and Alexa Fluor 488 goat antihuman IgG (FITC-IgG, 150 000 g·mol^{-1}) were obtained from Molecular Probes, Invitrogen. MTT and FDA/PI fluorescence staining assay kits were purchased from Sigma-Aldrich. NaCl and $CaCl_2$·$2H_2O$ (biotechnology grade) were purchased from Lach-ner, s.r.o (Neratovice, Czech Republic).

Synthesis of Polymers. *Quaternized Chitosan (CQM, CQH).* *N*-((2-Hydroxy-3-trimethylammonium)propyl) chitosan salts, commonly known as quaternized chitosan, were synthesized through the reaction between chitosan and GTMAC under acidic conditions, following the procedure described by Heydari et al.[35]

Quaternized Dextran (DQM). *O*-((2-Hydroxy-3-trimethylammonium)propyl) dextran salt, commonly known as quaternized dextran, with an average degree of substitution (DS) of 0.34 was synthesized by the reaction between dextran and GTMAC under basic conditions according to the procedure described by Heydari et al.[35]

Polyampholyte Chitosan (CAM). *N*-(3-Sulfopropyl) chitosan salt, denoted as polyampholyte chitosan, was synthesized by reacting chitosan with PrS under neutral conditions,[36] resulting in DS of 0.61.

Poly[(2-methyl-2-oxazoline)-co-(ethylene imine)] (POX). The statistical copolymer POX was prepared by a two-step synthesis, including the living cationic ring-opening polymerization of 2-methyl-2-oxazoline followed by partial acidic hydrolysis of the obtained poly(2-methyl-2-oxazoline) using the conditions providing 18 mol % of ethylene imine units.[37]

Sodium Cellulose Sulfate (SCS). The synthesis of SCS was based on the method of Schweiger.[38] In a typical experiment, cellulose (Whatman paper 1450-917, nondried, cut to ca. 0.5 × 0.5 cm pieces; 4.313 g, 26.6 mmol) was mixed with dried DMF (121 mL) in a 1000 mL jacketed reactor equipped with a powerful mechanical stirrer and connected to an argon inlet, and the suspension was left standing overnight. Then, the mixture was water-cooled to ca. 15 °C, and the SO_3 stock solution in DMF (95 mL, 1.12 M, 106.4 mmol of SO_3; prepared from SO_3·DMF under inert conditions) was added to the reactor through a Teflon cannula, under an argon flow, at slow stirring (50 rpm). After the addition, the reactor was tightly closed, the stirring speed was increased to 250 rpm, and the cooled mixture was stirred for 3 h. The filter paper gradually disintegrated and dissolved

https://doi.org/10.1021/acs.biomac.4c00222
Biomacromolecules 2024, 25, 4118−4138

during the reaction, ultimately yielding a homogeneous gel-like, semitranslucent mixture. Afterward, a solution of sodium acetate (26.18 g, 0.3192 mol) in water (178 mL) was added to the reaction mixture, and the formed fine, white suspension was stirred at 500 rpm for 50 min. Then, the powdery solids were collected on a glass frit, successively extensively washed with acetone, 95% MeOH, and MeOH, and finally dried in a vacuum at 30 °C overnight. A white powdery product (14.662 g) was obtained. The DS value of 2.9 was determined from the elemental analysis of a sample of the product from which sodium sulfate was removed via rapid dialysis (4 × 30 min, MWCO = 1000 g·mol^{-1}) followed by freeze-drying; note that prolonged dialysis appears to lead to product degradation (including loss of sulfate groups). The formula DS = 2.25 × (S/C) was used for the calculation, where S and C are wt % of sulfur and carbon, respectively, determined by the elemental analysis. Note that the product contains sodium sulfate originating from the neutralization of the residual SO_3. The content of sodium sulfate of 27 wt % was calculated by comparing the elemental analysis data of the nondialyzed and dialyzed products.

Poly(methylene-co-cyanoguanidine) (PMCG). PMCG was prepared according to the method of Zang and Li[39] with some modifications. In short, formalin solution, freshly prepared from 7.330 g (0.232 mol) of paraformaldehyde and 13.5 mL of water, was added to a 100 mL flask containing 1-cyanoguanidine (13 g, 0.155 mol) and ammonium chloride (8.27 g, 0.155 mol). The mixture was stirred at 80 °C for 3 h. Afterward, the clear solution was cooled down to room temperature, and the product was precipitated in 30-fold (v/v) excess of isopropyl alcohol, collected on a glass frit, washed thoroughly with isopropyl alcohol, and dried in a vacuum at 50 °C. The M_w of ∼3000 g·mol^{-1} was determined by SEC-MALS.

FITC-Labeling of Polymers. FITC-labeled CQM, CHM, and CAM chitosan derivatives were prepared according to Son et al.[40] Briefly, a polymer (0.1 g) was dissolved in 0.5 mol·L^{-1} aqueous solution of Na_2CO_3 (9 mL), and FITC (5 mg, 0.013 mmol), dissolved in 0.5 mol·L^{-1} Na_2CO_3 (1 mL), was added dropwise to this polymer solution. The reaction proceeded under stirring at room temperature for 24 h. FITC-labeled DQM and SCS were prepared according to the published procedure.[41] Shortly, a polymer (0.1 g), FITC (0.01 g, 0.026 mmol), pyridine (40 μL, 0.5 mmol), and dibutyltin dilaurate (8 μL, 0.01 mmol) were dissolved in dimethyl sulfoxide (DMSO, 10 mL). The reaction proceeded at 90 °C for 4 h. FITC-labeled POX was prepared as follows: POX (0.1 g) and $NaHCO_3$ (0.173 g, 2.05 mmol) were dissolved in 10 mL of water. Then, FITC (5 mg, 0.013 mmol) dissolved in DMSO (3 mL) was added dropwise to the POX solution, and the reaction mixture was stirred overnight at room temperature. All the FITC-labeled polymers were dialyzed against water (MWCO of 1000 g·mol^{-1}), and products were isolated by freeze-drying. All the synthesis and isolation steps were performed in the dark.

Preparation of PMCG Microcapsules. PMCG microcapsules were formed by polyelectrolyte complexation between polyanions (SA and SCS) contained in the polyanion (PA) solution and a polycation (PMCG) in the polycation (PC) solution, with the latter solution also containing the SA-gelling ions, following the procedure described previously[32] with some modifications. The PA solution contained 0.81 wt % SA and 0.88 wt % SCS dissolved in 0.9 wt % NaCl solution. The PC solution contained 1.5 wt % PMCG, 1 wt % $CaCl_2$, and 0.9 wt % NaCl. The pH of both the solutions was adjusted to 7.4, and the solutions were filter-sterilized using a 0.22 μm cellulose acetate syringe filter and bottle-top filters for PA and PC solutions, respectively. Filtration and microcapsule preparation were performed under sterile conditions in a laminar flow hood.

The PA solution was air-stripped at a flow rate of 0.60 ± 0.05 g·min^{-1} using a custom-designed coaxial nozzle to generate microcapsules with a diameter of about 900 μm. The resulting droplets were allowed to fall into a PC solution flowing in a glass multiloop reactor,[42] consisting of 7 loops with an inner diameter of 5 mm and a loop diameter of 11 cm, at a flow rate of 47 ± 1 g·min^{-1}. The gelling reaction time was maintained at 50 ± 4 s, which was achieved by controlling the microcapsule residence time in the multiloop reactor. The microcapsules were then collected at the end of the reactor in a beaker with 150 mL of a washing solution (WS), containing 0.022 wt % $CaCl_2$ (2 mmol·L^{-1}) and 0.9 wt % NaCl solution (pH adjusted to 7.4), to quench the gelling reaction. The WS was replaced at 1 min intervals, and the microcapsules were washed three times with 150 mL of WS using a stainless-steel sieve after each collection to ensure an effective exchange of solutions between the washing steps. The prepared PMCG microcapsules were divided into seven aliquots, with six aliquots subjected to postmodification and the remaining one used as a control (parent PMCG microcapsules).

Postmodification of PMCG Microcapsules. The postmodification was performed for 10 min at ambient temperature through gentle mixing of PMCG microcapsules in solutions containing 0.2 wt % of respective polyelectrolytes (PEs) dissolved in 0.9 wt % NaCl with pH adjusted to 7.4, at a microcapsules-to-polymer solution volume ratio of 1:20. Microcapsules were then washed three times with WS. The prepared postmodified microcapsules were either stored in WS in the fridge (denoted as "after preparation"), stored in the CMRL medium at 37 °C for 2 weeks, or shipped in WS to CellTrans, Inc., Chicago, for the intraperitoneal implantation to C57BL/6 mice. These microcapsules were retrieved 2 weeks postimplantation and shipped in WS back to the Polymer Institute SAS for characterization (marked as "after retrieval"). The microcapsules were characterized in WS (for microcapsules after preparation and after retrieval) or in CMRL (the CMRL-treated microcapsules).

Size-Exclusion Chromatography. The molar weights, MW, molar weight distributions, MWD, and dispersity, $Đ$, of polymers used for the preparation and postmodification of microcapsules were obtained by the aqueous-phase SEC-MALS. The conditions established for the characterization of polyanions[34,43] were used to characterize SA, SCS, and CAM, whereas the conditions established for the characterization of polycations[35,44] were used to characterize CQM, CQH, DQM, POX, and PMCG polymers. The refractive index increment, dn/dc, values were obtained via an online measurement using the WinGPC Unichrom routine (Polymer Standards Service, Mainz): SA 0.149 mL·g^{-1},[34] SCS 0.063 mL·g^{-1}, CAM 0.120 mL·g^{-1}, CQM and CQH 0.187 mL·g^{-1},[35] DQM 0.151 mL·g^{-1}, POX 0.182 mL·g^{-1}, and PMCG 0.190 mL·g^{-1}.

NMR. NMR spectra were recorded on a Bruker Avance III HD-400 spectrometer at 25 °C.

Microcapsule Size and Membrane Thickness. The diameter and membrane thickness of microcapsules (n = 20) were measured using an optical microscope from Optika SRL (Ponteranica, Italy) equipped with a Moticam 1.3MP camera and a Motic Images Plus 2.0 software.

Compression Resistance. The mechanical stability of the microcapsules (n = 20) in a compression mode was evaluated as a force required to rupture a single microcapsule (in g) using a Texture Analyzer XTplus (Stable Micro Systems, Godalming, U.K.) equipped with a Texture Expert software. Microcapsules were exposed to the compression force applied by a mobile probe moving vertically at a speed of 0.5 mm·s^{-1}.

Spatial Distribution of Fluorescently Labeled Polymers in Microcapsules by CLSM. A confocal laser scanning microscopy (CLSM) microscope Zeiss LSM 510 (Carl Zeiss, Jena, Germany) equipped with a 10/0.45 NA Apochromat objective was used to evaluate the spatial distribution of FITC-fluorescently labeled polymers according to the previously reported protocol.[24] The fluorescence intensity across the equatorial cross-section of microcapsules ($n \geq 6$) was determined to evaluate the relative local concentration of labeled polymers. Microcapsules after preparation and after exposure to CMRL were analyzed in WS and in CMRL, respectively. To measure fluorescence intensity, an excitation wavelength of 488 nm and an emission wavelength of 505 nm were used. The raw data were normalized to the maximum intensity. The distance along the microcapsule diameter was calculated as a percentage of the diameter, ranging from 0 to 100% between the opposite edges of the microcapsule. The data were analyzed using ZEN software (Carl Zeiss, Jena, Germany) and smoothed using OriginPro (OriginLab Corp.).

https://doi.org/10.1021/acs.biomac.4c00222
Biomacromolecules 2024, 25, 4118−4138

Spatial Distribution of Polymers in Microcapsules by CRM. All experiments were performed on the WITec alpha300 R+ confocal microscope, which was equipped with the WITec UHTS300 spectrometers, at a controlled ambient temperature of 23 °C. The water immersion objective Carl Zeiss 20x/1NA was used for the analysis of microcapsules using the 785 nm laser line for the excitation of the Raman signal. The spectra collection time was typically in the range of 25 s using a line scan with the stepwise scanning of a step size from 1 to 20 μm, depending on the required level of resolution. The overall time to create the CRM intensity profile of the respective polymer along the equatorial microsphere cross-section was approximately 60 min. The Carl Zeiss 50x/0.8NA objective was used to analyze the polymers used for the postmodification in a powder form. The instrument was controlled by WITec Suite software. All other details of the CRM setup are provided in our previous work.[24]

The absolute SA, SCS, and PMCG concentrations in microcapsules were determined by adopting the calibration protocol established for SA.[24] Figure S1 shows typical Raman spectra for SCS and PMCG polymers in saline solutions (0.9 wt % NaCl) that were used for calibration. The spectra were first background-subtracted in WITec software using the sixth-order polynomial fit with an automatic noise filter set to 2. The range intervals without significant vibrations were used for the definition of the polynomial fit. Once the data were background-subtracted, the fitting models were used to extract data. The data ranges for background subtraction are shown in Table S1. Then, the characteristic peaks for SA, SCS, PMCG, and water were fitted by Gaussian curves within the ranges and parameters for the fitting models contained in Table S2.

The calibration solutions were made in saline in the concentration ranges from 0.1 to 3.0 wt % and from 1 to 3 wt % for SCS and PMCG, respectively. The CRM spectra were acquired from solutions placed in a Petri dish. The signal was gathered by the direct immersion of the objective into the solution. Between 64 and 128 sampling points were used with the exposure time between 5 and 25 s. The details of these measurements are contained in Table S3. The concentrations were evaluated from each Raman spectrum using the areas obtained from fitting models by the normalization of the area of the characteristic peak of a given polymer to the area of the water-bending peak.[24] Such a normalized area was used to create a linear equation correlating the normalized area with concentration. The medians of normalized peak areas for every concentration were fitted with a linear function (Table S4). Linear fits of percentiles (5 and 95%) for each concentration were employed as confidence bands for the error evaluation of the concentration of polymers SA, SCS, and PMCG. For determining the absolute concentrations of these polymers in microcapsules, the same sixth polynomial model was used as described above. After the background subtraction, the spectra of microcapsules were evaluated with a slight modification of the ranges of interest for SA and PMCG polymers compared to those used for calibration in order to limit the interference due to a higher number of peaks in spectra of microcapsules compared to those for individual polymers. For PMCG, a summation of two Gaussian curves was used to fit the data in the region of interest since this region contains vibrations from both PMCG and SCS. Table S5 shows the data ranges and conditions used for determining the absolute concentrations of individual base polymers present in PMCG microcapsules.

FITC-IgG Permeability Assay and Spatial Distribution of Labeled PEs by CLSM. To evaluate the penetration of FITC-IgG into the interior of microcapsules, microcapsules (n = 6) were incubated for 24 h at 37 °C in 1 mL of a solution containing 20 μg·mL^{-1} of FITC-IgG, 0.9 wt % NaCl, and 0.022 wt % $CaCl_2 \cdot H_2O$ at pH 7.4. The fluorescence intensity was determined by CLSM at the equatorial cross-section using the excitation and emission wavelengths of 488 and 505 nm, respectively. Identical CLSM setup and method were used for the visualization of fluorescently labeled PEs.

Molar Weight Cutoff by Inverse Size-Exclusion Chromatography. The molar weight cutoff (MWCO) for selected microcapsules after their preparation and after the CMRL treatment was determined by inverse size-exclusion chromatography (iSEC) following the principles[45] and experimental setup[46] described previously. In this study, the eluent consisted of 0.9 wt % NaCl, 0.022 wt % $CaCl_2$, and 200 ppm NaN_3 with pH adjusted to 7.4. Narrowly distributed pullulan standards (Polymer Standard Service, Mainz, Germany), with MW from 180 to 805 000 g·mol^{-1}, and dextran standards (American Polymer Standard Corp., Mentor), with MW from 1320 to 3 800 000 g·mol^{-1}, were dissolved in the eluent and injected at the concentration of 3 mg·mL^{-1} via the 100 μL loop onto the column formed by microcapsules (packed volume ∼8 mL) positioned in a glass column 10 × 250 mm (Omnifit, Cambridge, U.K.) fitted with an adjustable plunger on each side. The eluent flow rate was 0.2 mL·min^{-1}. The elution volume for each standard was determined as the volume at which 50% of the standard is eluted. These values were used to determine the chromatographic partition coefficients, K_{SEC}, for each standard. The calibration curve was created as a Boltzmann fit of $(1 - K_{SEC})$ vs molecular weight.[47] The MWCO value is determined from the calibration curve as the column exclusion limit.

Zeta Potential. The surface charge of microcapsules was measured using SurPASS 3 (Anton Paar GmbH, Austria) equipped with a cylindrical cell. The zeta potential of microcapsules in the "after preparation" stage was measured using 0.1 mol·L^{-1} NaCl as electrolyte solution under pressure between 200 and 600 bar at pH = 7.4. To remove all salts remaining on the microcapsules and equilibrate with the measuring media, 0.5 g of microcapsules were three times rinsed with 50 mL of 100 mmol·L^{-1} NaCl solution before measurement. The permeability index of samples during the measurement was adjusted to 100 by changing the number of microcapsules for each sample. The zeta potential (mV) is reported as mean ± standard deviation (SD) (n = 10).

2D Sodium Dodecyl Sulfate-Polyacrylamide Gel Electrophoresis. For focusing, 0.4 μg of the monoclonal antibody in a volume of 1 μL was mixed with 110.5 μL of IEF buffer 1 (7 mol·L^{-1} urea, 2 mol·L^{-1} thiourea, 40 mmol·L^{-1} Tris, 1% ASB14, 1% Triton X-100), 1.5 μL of 3−10 NL IPG buffer (GE Healthcare), 4.0 μL of DeStreak (GE Healthcare), and 3 μL of 1% bromophenol blue. The mixture was used to hydrate a 7 cm pH 3−10 NL Immobiline Drystrip (GE Healthcare) for 12 h. After hydration, the strip was loaded in the Ettan IPG Phore 3 (GE Healthcare) and focused using the following program: step 300 V/4 h, gradient 300−1000 V/1 h, step 1000 V/1 h, gradient 1000−3000 V/3 h, step 3000 V/1.5 h, gradient 3000−5000 V/2.5 h, and a final step of 5000 V/3 h.

The proteins in the strip were then reduced and alkylated by subsequent 15 min incubations in DTT (10 mg·mL^{-1}) and IAA (37.5 mg·mL^{-1}) dissolved in an equilibration buffer (6 mol·L^{-1} urea, 2% SDS, 30% glycerol, 1.5 mol·L^{-1} Tris-HCl pH 8.8). The strip was then placed on the top of a 11% acrylamide-bis-acrylamide gel, fixed in place with a mixture of 0.5% agarose and bromophenol blue in ELFO buffer (25 mmol·L^{-1} Tris, 192 mmol·L^{-1} glycine, 0.1% SDS) and ran at 15 mA until the blue tracer was released from the gel. The spots were revealed by SYPRO ruby (Invitrogen) staining. The stained gel was scanned using a Pharos FX scanner (Bio-Rad), and the molar weight and pI of the spots were calculated using the ImageMaster 2D platinum software (Amersham) and the 2D SDS-PAGE standards from Bio-Rad ran under the same conditions.

***β*TC3 Cell Encapsulation.** *β*TC3 pancreatic mouse cells (DSMZ, Braunschweig, Germany) were washed with saline solution and centrifuged at 1500 rpm for 1 min. The supernatant was removed and the cells were collected and resuspended in the PA solution at a density of 1 × 10^6 cell·mL^{-1}. Then, microcapsules were prepared and postmodified as described above for empty microcapsules. The encapsulated cells were cultured in the DMEM medium supplemented with 15% HSA, 2.5% FBS, and 1% penicillin/streptomycin at 37 °C under 5% CO_2. The cell proliferation and viability from day 1 to day 28 were assessed by MTT assay and fluorescein diacetate-propidium iodide (FDI/PI) staining.

The MTT assay was performed as follows: 20 microcapsules were incubated in 200 μL of MTT for 3 h. Afterward, microcapsules were washed with phosphate-buffered saline (PBS), PBS was aspirated, and 200 μL of DMSO was added to the microcapsules. The microcapsules were then incubated on an orbital shaker for 15 min to extract

https://doi.org/10.1021/acs.biomac.4c00222
Biomacromolecules 2024, 25, 4118−4138

formazan from the encapsulated cells. 100 μL aliquots of the supernatant were taken to a new 96-well plate and optical density (OD) at 595 nm was measured using a microplate reader Multiskan FC (Thermo Fisher Scientific). Data were analyzed using MARS Data Analysis software SkanIt. The FDA/PI fluorescence staining was used for determining the viability of encapsulated cells according to the protocol established by Shalaby et al.[48] Around 20 microcapsules with encapsulated βTC3 cells were added to 1 mL of FDA/PI solution and incubated at ambient temperature for 15 min in the dark. Then, microcapsules were washed with saline solution and assessed by fluorescence microscopy (Optika Microscopes, mercury lamp) equipped with a camera (Canon 350D). The DAPI UV filter was used to visualize the fluorescent green (alive) and red (dead) cells.

Implantation of Microcapsules. 500 μL of microcapsules of each type were implanted into the intraperitoneal (IP) cavity of immunocompetent C57BL/6 mice (n = 4 per microcapsule type) using the previously described procedure.[24] Microcapsules were retrieved 2 weeks postimplantation, placed into WS, and used for PFO evaluation and other analyses. The images of retrieved microcapsules (n = 100 microcapsules per mouse) were assessed using Cell^{3}imager software.[13] Based on the percentage of the microcapsule surface area covered by PFO, the microcapsules were divided into four categories (0−25, 26−50, 51−75, 76−100%). All animal care procedures were followed under the protocol approved by the Institutional Animal Care and Use Committee (IACUC) at the University of Illinois-Chicago (UIC).

Human Whole Blood Assay. The *in vitro* immunogenicity of the empty microcapsule was evaluated using a human whole blood assay (WBA). 500 μL of whole blood from healthy donors (n = 3), anticoagulated with lepirudin, was added to 50 μL of each type of microcapsules, to a saline solution used as a negative control, and to *Escherichia coli* used as a positive control, followed by incubation for 4 h at 37 °C.[21,29] EDTA (10 mmol·L^{-1}) was then added to stop the reaction, and samples were centrifuged at 3000 rpm for 15 min at 4 °C. Plasma was collected and stored at −20 °C for further study of complement activation and induction of inflammatory mediators. The alginate-poly-L-lysine (SA-PLL) microcapsules and sodium alginate beads (SA-beads), prepared according to the methods described by Rokstad et al.,[29] were used for a comparison with PMCG-type microcapsules.

Cytokine Induction. The following cytokines were determined in plasma samples using a Bio-Plex Human Cytokine 27-Plex Panel (Bio-Rad, Hercules, California): Interleukin IL-1β, IL-1RA, IL-2, IL-4, IL-5, IL-6, IL-8 (CXCL8), IL-10, IL-17, Eotaxin-1 (CCL11), fibroblast growth factor (FGF), granulocyte colony-stimulating factor (G-CSF), granulocyte macrophage-colony-stimulating factor (GM-CSF), interferon-γ (IFN-γ), monocyte chemoattractant protein-1 (MCP-1, CCL2), macrophage inflammatory protein-α (MIP-1α, CCL3), tumor necrosis factor-α (TNF-α), and vascular endothelial growth factor (VEGF).

Complement Activation. The soluble terminal complement complex (TCC) in plasma was measured using an ELISA kit for Human Terminal Complement Complex (Hycult Biotech, Uden, Netherlands).

CD11b Expression. CD11b expression was measured after incubating the microcapsules in lepirudin-anticoagulated human whole blood for 60 min. PE anti-CD11b and the nuclear dye LDS-751 were used to stain CD11b in granulocytes and monocytes and then were measured using a flow cytometer (Beckman Coulter Epics XL-MCL, Coulter Corp, FL).

Statistical Analysis. A statistical comparison of the data was performed using one-way analysis of variance (ANOVA) and Tukey's post hoc test for comparison of more than two groups. Differences with $p < 0.05$ were considered to be statistically significant.

RESULTS AND DISCUSSION

PE and Microcapsule Preparation. In this work, we aimed to prepare the parent PMCG microcapsules from well-defined starting materials. To this end, we combined the commercially available medium viscosity ultrapure SA with newly synthesized SCS and PMCG that replaced the previously used commercial alternatives that were either discontinued (SCS) or suffered from batch-to-batch variability (PMCG). The PMCG microcapsules were prepared according to a published protocol[32] with minor changes as detailed in the experimental section. Subsequently, these parent PMCG microcapsules were postmodified by immersion in 0.2 wt % solutions of different PEs. The postmodification conditions were selected considering the previous literature reports[11,49] and our preliminary trials on the detectability of PEs by the used characterization methods.

A library of PEs was prepared through established synthetic protocols and included both synthetic and semisynthetic (polysaccharide-based) PEs differing in their monomeric unit structure, charge type and density, and molar weight (MW) (Table 1, Scheme 1). MW values of these PEs were obtained by size-exclusion chromatography using multiangle laser-light scattering and refractive index detectors (SEC-MALS); the corresponding MW distributions are shown in Figure S2.

Table 1. Characteristics of the PEs Used for the Postmodification of PMCG Microcapsules

code	polymer	ionized group (DS)[a]	M_w[b]·10^{-3} (g·mol^{-1})	$Đ$[b]
CQM	quaternized chitosan, medium DS	quaternary ammonium (0.52)	100	1.9
CQH	quaternized chitosan, high DS	quaternary ammonium (1.06)	130	1.7
DQM	quaternized dextran	quaternary ammonium (0.34)	120	2.3
POX	poly[(2-methyl-2-oxazoline)-*co*-(ethylene imine)]	secondary amine (0.18)	10	1.5
CAM	ampholytic chitosan	sulfonate (0.61)	110	1.8
SCS	sodium cellulose sulfate	sulfate (2.9)	1030	1.8

[a]Degree of substitution (DS) defined as the number of ionized groups (at pH 7.4) per monomeric unit. For POX, the approximate fraction of hydrolyzed monomeric units is provided instead. [b]Weight-average molar weight and dispersity determined by SEC-MALS.

CQH and CQM were synthesized by the quaternization of chitosan of medium MW, introducing, on average, a quaternary ammonium group on every or every other sugar repeat unit, respectively.[35] DQM is a dextran derivative[35] of a similar MW as CQM and CQH but with comparatively lower charge density, featuring the quaternary ammonium group approximately on every third repeat unit. The polyampholyte CAM is a medium-MW chitosan derivative featuring sulfopropyl groups.[36] Note that the primary/secondary amine groups in chitosan-based PEs may potentially contribute to the overall charge, with the extent of this contribution influenced by the used conditions (pH, salt concentration). For CQM and CQH, these charge regulation effects will suppress the amine group ionization while for CAM the ionization will be enhanced.[50] Nevertheless, we expect CAM to retain a negative net charge under the used conditions. SCS is a high-MW polysaccharide-based polyanion of MW ∼ 10^6 g·mol^{-1} and approximately three sulfate groups per each anhydroglucose repeat unit; therefore, the average content of anionic groups in the repeat unit is approximately five times higher than for

https://doi.org/10.1021/acs.biomac.4c00222
Biomacromolecules 2024, 25, 4118−4138

Scheme 1. Representative Structures of PEs Used for the Preparation of PMCG Microcapsules and Their Postmodification

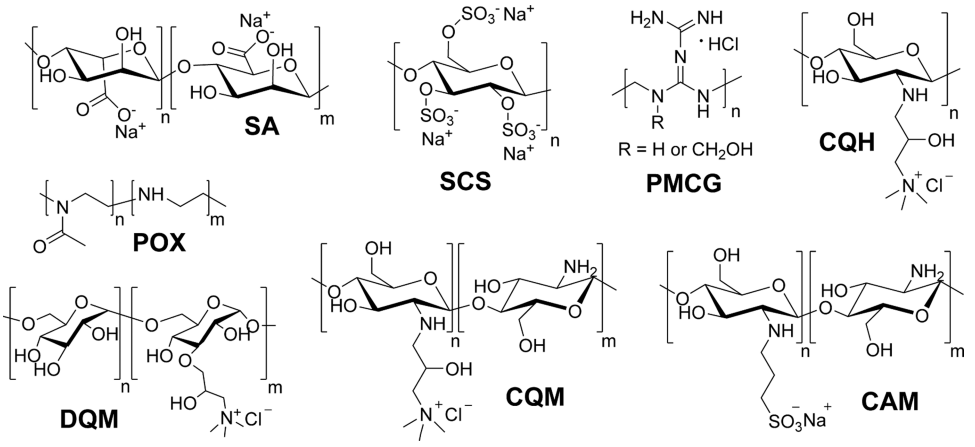

CAM. Note that an identical SCS polymer was used for both preparation and postmodification of PMCG microcapsules. POX is a synthetic polycation that features secondary amine groups as ionizable moieties and has a significantly lower MW compared to the polysaccharide-based polycations studied here. The thorough characterization of some of the used polymers (CQM, CQH, DQM, CAM) is provided in our recent papers.[35,36] NMR spectra of the remaining synthesized polymers used in this study are provided in Figure S3.

Both the parent and postmodified microcapsules were subsequently studied *in vitro* by a range of techniques in order to establish the impact of the postmodification on various microcapsule characteristics, including size, membrane thickness, compression resistance, surface charge, spatial distribution of polymers, permeability, viability of encapsulated cells, complement activation, and cytokine induction. In addition, a fraction of the prepared microcapsules was implanted into the peritoneal cavity of C57BL/6 mice for 2 weeks to examine how the postmodification influences the microcapsule biocompatibility characterized by the extent of PFO in retrieved microcapsules. We also obtained limited characterization data for these explanted microcapsules to provide additional insights into their *in vivo* performance.

Physical Characterization of Microcapsules. Figure 1 reveals the effect of postmodification on microcapsule size, membrane thickness, and compression resistance for microcapsules after preparation and after retrieval from the mouse model. Note that for PMCG microcapsules, the term membrane traditionally refers to the outer shell of the microcapsule, the thickness of which is determined using optical microscopy images where the distance between the microcapsule surface and the dark/bright interface line is measured. The remaining (inner) part of the microcapsule is then denoted as the core (see Figure S4). For microcapsules where the interface separating the core and the membrane becomes diffuse or multiple interfaces are present, the membrane thickness determination may become less accurate and more operator-dependent. Note that membrane thickness could not be evaluated for SCS-postmodified microcapsules after their retrieval from mice due to the strong PFO (Figure 1d).

The average diameter of the postmodified microcapsules (determined at the "after preparation" stage) remained very close to that of the parent microcapsules (Figure 1a). In the majority of cases, the *in vivo* environment induced slight microcapsule swelling, as evidenced by the registered microcapsule size values at the "after retrieval" stage. An exception was microcapsules postmodified with POX, whose average diameter remained virtually unchanged, and with SCS that shrank noticeably. However, the recorded size changes were generally rather minor.

More pronounced were the changes observed in membrane thickness (Figure 1b). After preparation, the membrane thickness of the studied microcapsules was in a relatively narrow range of ca. 0.07−0.09 mm, with the parent PMCG microcapsule in the middle of this range at 0.08 mm. The exposure to the *in vivo* environment triggered an increase in membrane thickness for all microcapsules for which this parameter could be evaluated. While this increase was relatively minor for some microcapsules (e.g., CQH-postmodified), it was substantial in other cases (e.g., ca. 35% for the parent PMCG microcapsule). However, the evaluation of membrane thickness for some of the microcapsules, particularly the explanted ones, was difficult due to the complex character of the membrane-core interface as noted above.

The most significant developments were registered for compression resistance (Figure 1c), quantified using a Texture Analyzer as a force (in grams) required to rupture a single microcapsule.

When evaluated at the "after preparation" stage, the postmodification had an insignificant impact on microcapsule mechanical stability as the compression resistance of postmodified microcapsules remained within approximately 15% of the value recorded for the parent microcapsule. However, the *in vivo* environment triggered a significant drop in compression resistance values across the board, with the magnitude of this decrease being very different for individual microcapsules. Remarkably, the postmodification played a crucial role in maintaining mechanical resistance for CQM- and DQM-postmodified microcapsules that both showed compression resistance of ca. 20 g after retrieval. This effect was not necessarily related to the high initial (after preparation) values of compression resistance. For example, the CQH-postmodified microcapsules, which showed one of the highest values of compression resistance after preparation, were found to be rather fragile after retrieval (a decrease from 29 to 8 g). Strikingly, after retrieval, the mechanically weakest microcapsules (~5 g) were the variants postmodified with negatively charged PEs, CAM, and SCS, despite them showing compression resistance levels similar to that of the parent

https://doi.org/10.1021/acs.biomac.4c00222
Biomacromolecules 2024, 25, 4118−4138

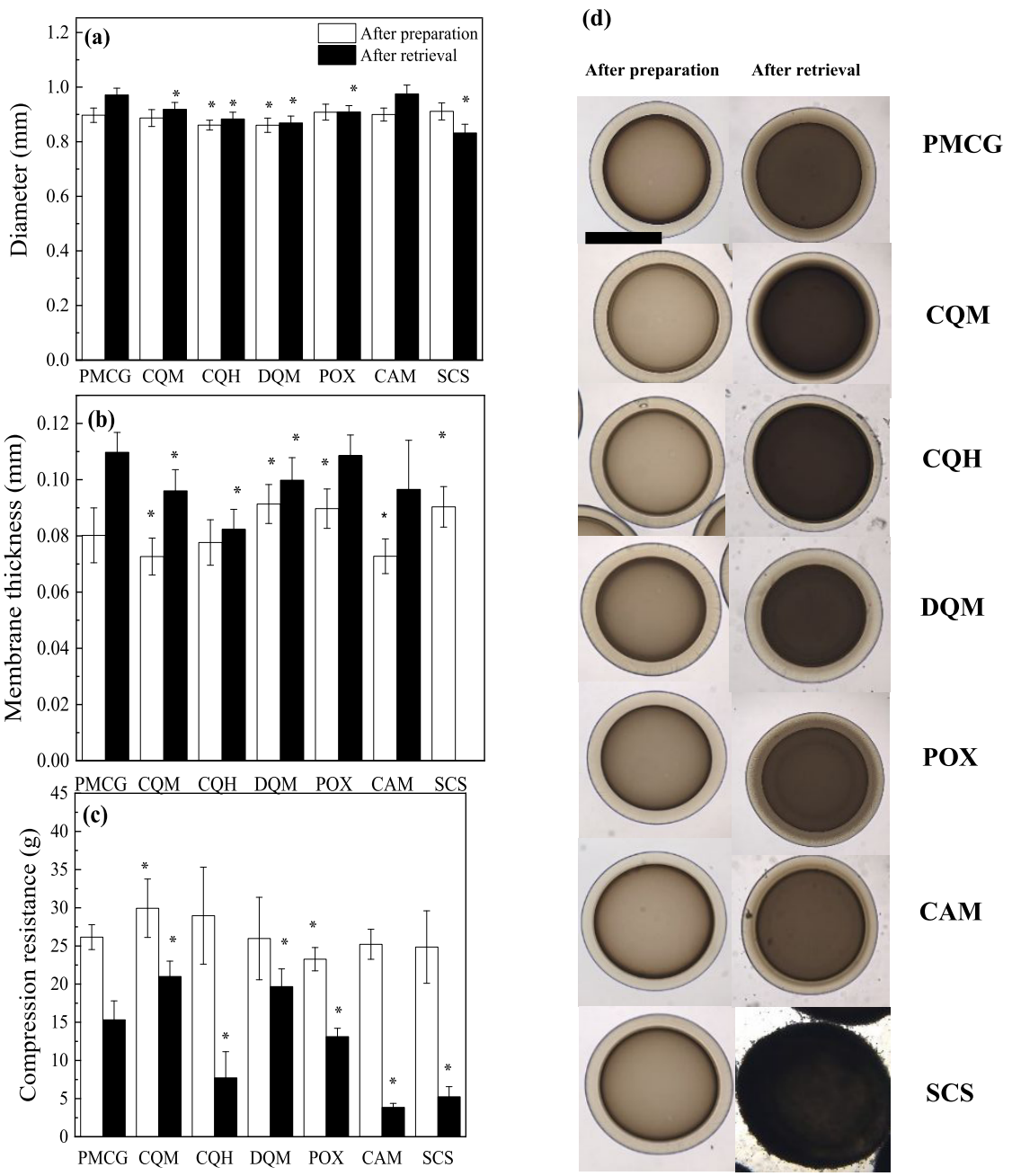

Figure 1. (a) Size, (b) membrane thickness, and (c) compression resistance of microcapsules after preparation and after retrieval from the peritoneal cavity of C57BL/6 mice. Data are mean ± SD (n = 20 microcapsules per batch). PMCG stands for the parent PMCG microcapsules. Optical microscopy images of microcapsules (d) after preparation and after retrieval. Bar equals to 500 μm. Statistical comparison is done between postmodified vs parent PMCG microcapsules, * $P < 0.05$.

PMCG microcapsule after preparation. The finding that the PMCG microcapsules can be mechanically reinforced through postmodification with specific PEs holds high practical significance as the *in vivo* environment is often challenging to the integrity of implanted microspheres.[51]

Figure 1d provides the optical microscopy images of the parent and postmodified PMCG microcapsules at both the stages studied. Note that darkening of the core and/or the interface between the core and the membrane are typical features of PMCG microcapsules exposed to *in vivo* conditions.[17]

Microcapsule Biocompatibility. In order to assess the impact of postmodification on microcapsule biocompatibility, i.e., the lack of fibrotic overgrowth, microcapsules were implanted into the intraperitoneal cavity of immunocompetent C57BL/6 mice. This mouse model is considered to be suitable for mimicking the PFO observed in both humans and NHPs.[52] The fibrotic response to implanted microcapsules was evaluated by the visual inspection of retrieved microcapsules and categorization with respect to PFO degree. The images of retrieved microcapsules (n = 100 microcapsules per mouse) were assessed using an image analysis software,[13] where the microcapsules were divided into four categories corresponding to the percentage of their surface area covered by PFO: 0−25, 25−50, 50−75, 75−100%. The distribution of microcapsules in these categories is visualized as pie charts in Figure 2, with

https://doi.org/10.1021/acs.biomac.4c00222
Biomacromolecules 2024, 25, 4118−4138

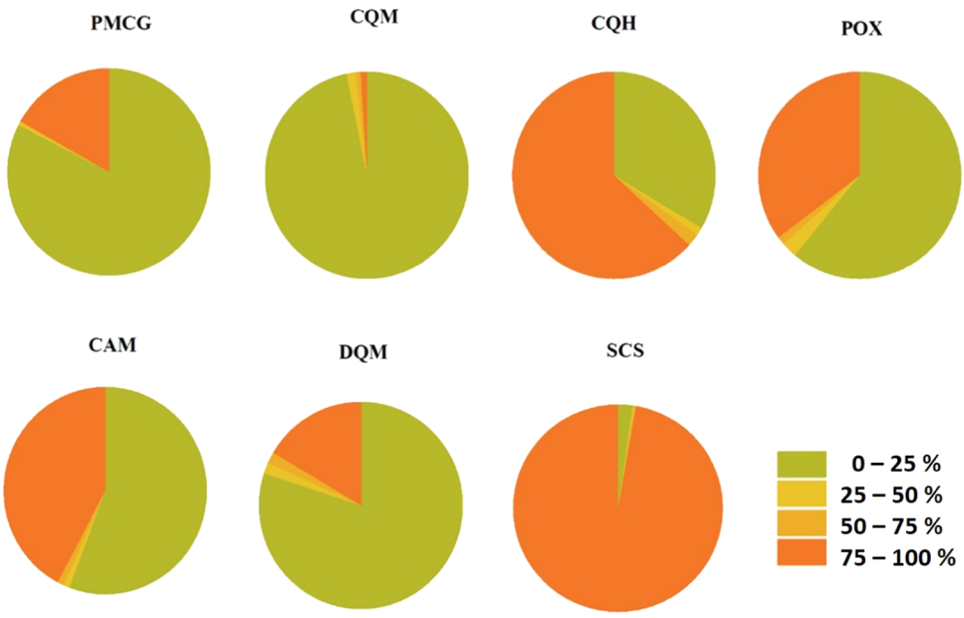

Figure 2. Pie charts depicting the distribution of microcapsules in the four defined PFO categories in the parent and postmodified PMCG microcapsules (n = 100 per animal) retrieved 2 weeks postimplantation from the peritoneal cavity of C57BL/6 mice (n = 4 animals).

histograms facilitating quantitative evaluation provided in Figure S5. Focusing on the fraction of the heavily overgrown microcapsules (the 75−100% PFO category), the data show that the parent PMCG microcapsule triggered severe fibrosis on close to 20% of microcapsules. DQM-postmodified microcapsules showed a very similar result while most of the remaining postmodified microcapsules fared considerably worse, exhibiting a considerable proportion of heavily overgrown microcapsules. The PFO was particularly severe for SCS, for which approximately 95% of microcapsules fell into the 75−100% PFO category. Most importantly, however, the postmodification of the parent PMCG microcapsule with CQM largely mitigated the PFO as evidenced by the low content (ca. 4%) of heavily overgrown microcapsules in this particular sample.

Further, we note that there is almost complete absence of the intermediately overgrown microcapsules (the 25−50 and 50−75% PFO categories) in the retrieved samples (Figure S5). Although the main factor responsible for triggering the foreign body response is currently unknown, our findings suggest that the actual onset of PFO represents the rate-limiting step, with PFO progressing relatively rapidly afterward until a high degree of fibrotic coverage is reached. This leads to the characteristic observed pattern of overgrown microcapsules present alongside clean ones.

Interestingly, the excellent *in vivo* performance of CQM-postmodified microcapsules in terms of minimal PFO appears to align well with the previously discussed findings on the mechanical properties of explanted microcapsules where this particular microcapsule type also provided superior results. To study the potential relationship between these two seemingly distant characteristics, we plotted the percentage of little overgrown (0−25% PFO) and heavily overgrown (75−100% PFO) microcapsules against the average compression resistance of the given microcapsule type (Figure S6). In both cases, there appears to be an apparent correlation, i.e., the microcapsules that remained mechanically strong when exposed to the *in vivo* environment also showed higher biocompatibility, while the weakened ones exhibited a significant degree of PFO. The potential causative factors behind this relationship remain presently uncertain. For example, it can be speculated that the formation of a fibrotic layer on the microcapsule surface deteriorates the mechanical properties of microcapsules by facilitating crack nucleation/propagation.[53] On the other hand, it is also known that the mechanical properties (e.g., modulus) of a hydrogel material can influence its biocompatibility.[54] Of course, both enhanced biocompatibility and compression resistance could simply be related to another factor. For instance, the postmodification with a suitable PE could potentially both reinforce the IPEC network within the microcapsule structure and affect other structural features, e.g., surface properties, relevant to the PFO. Even though the underlying factors remain unclear, the observation that microcapsule postmodification with a PE can improve both its mechanical stability and biocompatibility provides important support to this strategy. It is also interesting that polycations, previously frequently shown to enhance inflammatory responses,[28,29,31] were most effective in this sense, highlighting that different PE types may be suitable for enhancing the mechanical properties and biocompatibility of different microsphere types. Nevertheless, it should be emphasized that former studies relied mostly on PLL as the polycation, and the different PEs used here could mount different outcomes. In the following sections, we applied various techniques to study which factors could potentially contribute to the observed differences in the behavior of postmodified microcapsules.

Microcapsule Permeability. Next, we sought to obtain an insight into microcapsule permeability. Because the relationship of this parameter to microsphere biocompatibility and immunoprotective function is complex,[10] we use here the permeability assessment solely as an additional probe into the postmodification-associated structural changes in microcapsules. That is, we assume that the detected differences in permeability reflect the structure of the hydrogel material in terms of network density and PE localization and,

https://doi.org/10.1021/acs.biomac.4c00222
Biomacromolecules 2024, 25, 4118−4138

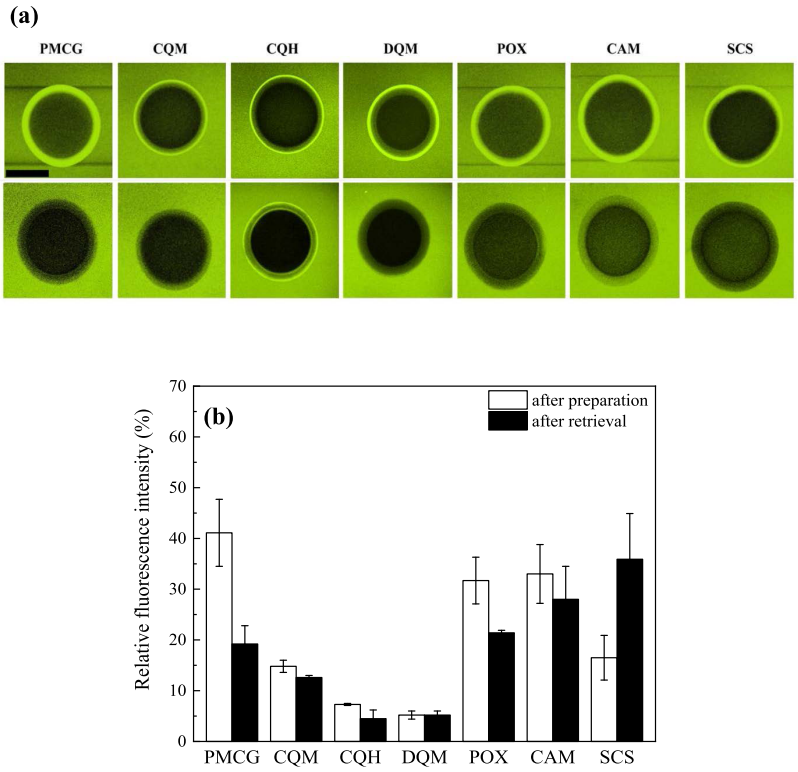

Figure 3. Permeation of FITC-IgG to microcapsules for parent and PE-postmodified PMCG microcapsules: (a) CLSM images visualizing the spatial distribution of FITC-IgG at the equatorial microcapsule cross-section for microcapsules after preparation (upper row) and after retrieval from C57BL/6 mice 2 weeks postimplantation (bottom row), bar is equal to 0.5 mm; and (b) relative fluorescence intensity of FITC-IgG in the microcapsule core relative to that in the surrounding IgG solution for microcapsules after preparation and after retrieval from C57BL/6 mice 2 weeks postimplantation.

consequently, also relate to factors such as surface properties that are potentially relevant to microcapsule performance (e.g., biocompatibility).

To study the microcapsule permeability toward charged species, we exposed the microcapsules to fluorescently (FTIC) labeled IgG. IgG is a polyclonal antibody characterized by MW of ~150 000 g·mol^{-1}, R_η ~ 5 nm, and weakly anionic net charge at the physiological pH as verified by 2D sodium dodecyl sulfate-polyacrylamide gel electrophoresis revealing predominantly fractions with pI < 7.4 (Figure S7). Importantly, in this permeability study, we were also able to utilize the microcapsules explanted from the mice model, which allowed for a direct comparison of the microcapsule properties in the "after preparation" and "after retrieval" stages.

As shown in Figure 3a, IgG tends to concentrate inside the membrane for microcapsules studied after their preparation, with different depths of penetration observed depending on the PE used for the postmodification. This is visually manifested by the relative increase in the fluorescence intensity within microcapsules as compared to the surrounding solution of labeled IgG. In general, IgG showed increased concentration in the whole membrane volume for the parent PMCG microcapsule as well as for the POX, CAM, and SCS-postmodified microcapsules. On the other hand, IgG concentrated only in the outermost membrane layer for the microcapsules postmodified with the high-MW polycations (CQM, CQH, DQM), possibly due to the more efficient IgG retention in the membrane. Presumably, the observed IgG accumulation pattern results from the interplay between the electrostatic interaction of IgG with polycationic microcapsule components (PMCG and polycationic polymers used for postmodification) and the local permeability of the hydrogel network. It has been shown previously for alginate microbeads[55−57] and PMCG microcapsules[55] that the release of entrapped proteins is controlled by electrostatic interactions rather than by microbead/microcapsule MWCO or protein MW. Nevertheless, we also cannot exclude the participation of other (non-Coulombic) interactions, especially when we consider the similar IgG uptake pattern for the parent and polyanion-postmodified microcapsules.

When the explanted microcapsules were studied in the same way, no IgG accumulation in the membrane was observed for the majority of microcapsules, indicating either the disappearance, spatial redistribution, or charge saturation of polymers interacting with IgG, or a significant decrease in membrane permeability. The only exception was the CQH-postmodified microcapsule where an onion-type pattern was observed, characterized by the increased IgG concentration at the outer and inner edges of the microcapsule membrane. This specific pattern indicates the increased local concentration of species (e.g., polycations) that attract IgG at the membrane boundaries.

Figure 3b depicts the relative fluorescence intensity in the microcapsule core in relation to the intensity of the surrounding labeled IgG solution. While none of the microcapsules studied were completely resistant to IgG penetration into the microcapsule core, significant differences could still be observed. Focusing first on microcapsules in the "after preparation" stage, the IgG permeation into the core was lower for all the postmodified microcapsules than for the

https://doi.org/10.1021/acs.biomac.4c00222
Biomacromolecules 2024, 25, 4118−4138

parent PMCG microcapsule. The IgG access to the core was limited particularly for the microcapsules postmodified with high-MW polycations, i.e., CQH, DQM, and partially also CQM (approximate relative intensity values of 5 to 15%). For most explanted microcapsules, the IgG uptake into the core tended to remain the same or further decrease, the exception being the SCS-postmodified microcapsules for which the observed relative fluorescence intensity doubled when compared to the "after preparation" stage. This considerably enhanced permeability indicates significant changes to the hydrogel network structure of the SCS-postmodified microcapsule. While this finding could help explain the previously observed poor mechanical stability of these microcapsules, the link to the also observed low biocompatibility is currently unclear. Overall, the obtained data show that the permeation of IgG to the core of PMCG microcapsules may be suppressed by postmodification, particularly with high-MW polycations.

To further improve our understanding of the effects underlying the observed IgG permeability data, we also performed the iSEC analysis of selected microcapsules to determine their MWCO. In iSEC, the tested microcapsules were used as a column packing, and a MWCO value was obtained as a column packing exclusion limit, expressed by the lowest MW of the solute fully excluded by the microcapsule material.[45,47] In iSEC, the solutes should be noninteracting with microcapsules and should separate only based on their size, which is fulfilled for the used pullulan and dextran standards.[46] Therefore, the electrostatic interaction, as one of the possible major forces modulating the permeation of IgG in the microcapsule material, is absent in iSEC as the method is based on the permeation of neutral molecules.

Herein, we studied the parent PMCG microcapsules alongside the CQM- and DQM-postmodified variants that represented the most promising microcapsule (from the perspective of biocompatibility and *in vivo* mechanical stability) and the least permeable microcapsule from the IgG assay, respectively. Besides studying the microcapsules in the "after preparation" stage, we also characterized microcapsules that were placed into the CMRL culture medium for 2 weeks in order to obtain data for microcapsules exposed to a more complex environment than the standard saline/$CaCl_2$ storage solution. CMRL medium is used to culture pancreatic islets before, as well as after, their encapsulation in alginate-based microspheres[58] and thus represents a relevant environment from an application point of view.

Figure S8 provides the elution curves of pullulan and dextran standards injected on the columns packed with the respective microcapsules. MWCO values obtained from the corresponding iSEC calibration curves shown in Figure S9 are then summarized in Table 2. Based on these data, two major observations can be made. First, the postmodification by CQM or DQM has a negligible influence on the MWCO of the microcapsule hydrogel material as indicated by the very similar determined MWCO values of around 120 000 g·mol^{-1}. This indicates that the postmodification may not have a significant impact on the base hydrogel network of the microcapsules, at least in the studied cases. Additionally, the insensitivity of MWCO (determined using neutral molecules) to polycation postmodification points to the important role of electrostatic interactions in the permeation behavior of labeled IgG discussed above. Second, the iSEC study revealed that the CMRL treatment inflicted a substantial drop in microcapsule permeability, as documented by the MWCO values decreasing to approximately half of the original ones upon the CMRL treatment. This difference is illustrated particularly well by the elution curves for standards with MW of 70 000 and 113 000 g·mol^{-1} that are close to the exclusion limit and show higher permeation in the case of the microcapsules after preparation compared to those after the exposure to CMRL (Figure S8). The MWCO values determined with the polysaccharide standards correspond to the exclusion limit expressed as a viscosity radius, R_η, of approximately 10 nm (after preparation) and 6 nm (after CMRL).[45] However, the MWCO values obtained by iSEC should be considered as approximate and not representative of a sharp cutoff limit (see the additional discussion accompanying Figure S8). Nevertheless, iSEC can still be considered as a useful method because it allows for microcapsule analysis under physiological conditions. The obtained results are consistent with those from the IgG permeation study in the sense that complex environments (*in vivo* or culture media) may significantly impact on the permeation of both charged and uncharged macromolecules within the microcapsule hydrogel material.

Table 2. MWCO Values for the Parent PMCG Microcapsule and Microcapsules Postmodified by CQM and DQM after Preparation and after Exposure to CMRL

	MWCO (g·mol^{-1})	
microcapsule type	after preparation	after exposure to CMRL
PMCG	110 000	60 000
DQM	130 000	65 000
CQM	110 000	50 000

Spatial Distribution of Polymers in Microcapsules. Key microcapsule properties, such as their compression resistance, permeability, or biocompatibility, are expected to be dependent on the localization of polymeric components within the microcapsule volume. Therefore, we applied two established methods, CRM and CLSM, to map the polymer spatial distribution within both parent and postmodified microcapsules. We sought to address two major questions: (i) how the postmodification impacts on the spatial distribution of the base polymers forming the parent PMCG microcapsule (i.e., SA, SCS, and PMCG), and (ii) where the PEs used for postmodification are localized. The first question is important from the perspective of revealing whether the postmodification with a PE (under the given conditions) has the potential to disrupt the IPECs present in the parent microcapsule that are thought to be responsible for the specific microcapsule properties distinguishing it from simpler systems such as alginate microbeads (e.g., mechanical resistance or the potentially tunable MWCO). The second question may then be relevant from the perspective of microcapsule biocompatibility, particularly when polycations are used.

First, we employed the CRM technique to study the effect of postmodification on the spatial distribution of the base polymers. In our previous paper, we introduced CRM as a tool for mapping polymers in alginate-based hydrogel microspheres, including PMCG microcapsules.[24] In the present study, we introduce a significant advancement in the application of this technique to multicomponent microcapsules, moving from the previously used relative concentration profiles to absolute concentration profiles, a step enabled by the calibration of the Raman signal intensity (Figure S1, Tables S1−S5). Figure 4 shows the spatial

https://doi.org/10.1021/acs.biomac.4c00222
Biomacromolecules 2024, 25, 4118−4138

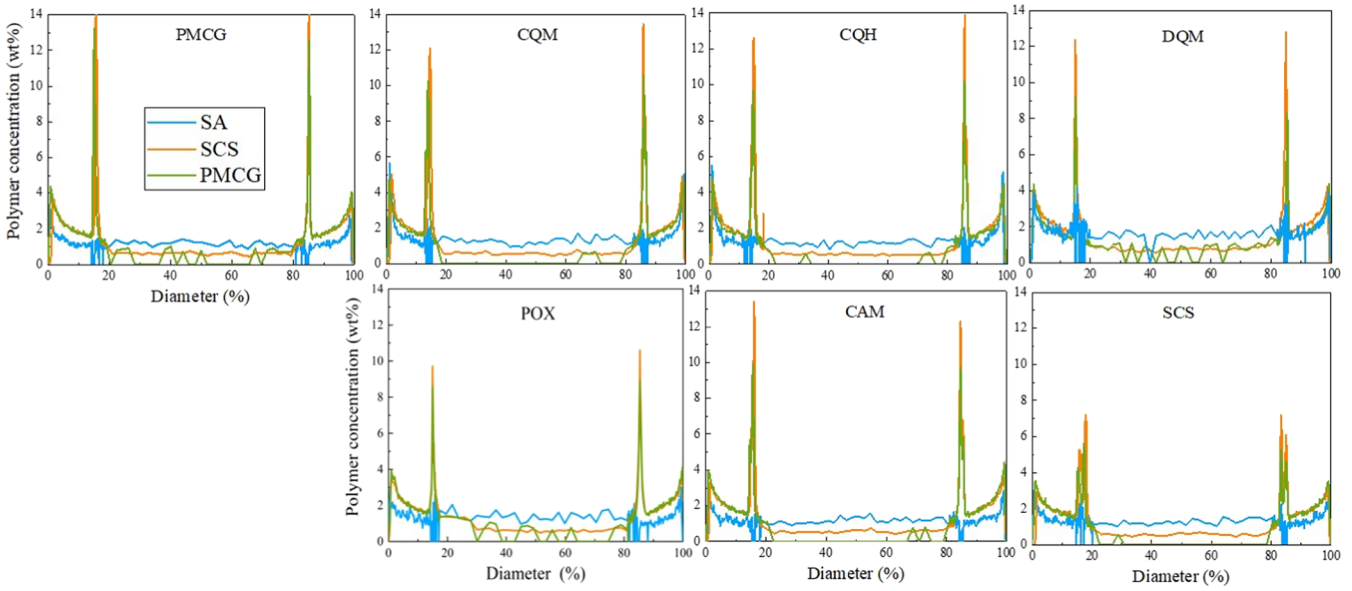

Figure 4. CRM profiles visualizing the concentration of the base PMCG microcapsule polymeric components (SA, SCS, and PMCG) at the equatorial microcapsule cross-section in the parent and postmodified PMCG microcapsules (at the "after preparation" stage) plotted against the diameter expressed as a percentage, where the microcapsule edges are located at 0 and 100% of the diameter.

distribution profiles of SA, SCS, and PMCG for all the studied microcapsule types (at the "after preparation" stage) plotted against the microcapsule diameter. The microcapsule diameter is expressed as a percentage, with the microcapsule edges located at 0 and 100% of the diameter. Using the normalized diameter value allowed us to account for the slight variation in microcapsule size.

Focusing first on the spatial distribution of polymers in the parent PMCG microcapsule, it is clear that all three polymers show local concentration maxima near the microcapsule surface. While this maximum is a global one for SA (ca. 3 wt %), both SCS and PMCG exhibit additional (global) maxima (ca. 12−14 wt %) between 10 and 20% of the diameter beneath the microcapsule surface. This position presumably corresponds to the layer of IPEC between SCS and PMCG created during the microcapsule fabrication. While it is tempting to equate this layer with the border of the microcapsule membrane observed in the optical microscopy images (Figure 1d), there appears to be a mismatch between the membrane thickness determined by optical microscopy (ca. 10% of the microcapsule diameter) and the IPEC layer localization (ca. 15% of the diameter). The CRM result would place the IPEC layer onto the inner side of the dark band region separating the microcapsule core and membrane (see Figure S4). Nevertheless, the insufficient precision of the determination of the boundary positions from both the CRM and optical microscopy data, as well as the variation in the microcapsule size and membrane thickness, did not allow us to precisely match the data obtained from different techniques. Further, the CRM analysis revealed that the microcapsule core predominantly consists of SA (ca. 1 wt %), with the presence of some SCS (ca. 0.5 wt %). On the other hand, PMCG is barely detectable within the microcapsule core.

The overall spatial distribution profile of polymers within the microcapsule volume corroborates the assumed mechanism of microcapsule formation, based on two parallel noncovalent cross-linking processes.[32] That is, when the polyanion solution droplet (containing SA and SCS) enters the gelling solution (containing Ca^{2+} and PMCG), the alginate hydrogel network is quickly formed through the penetration of the small Ca^{2+} ions into the droplet volume (hence the slight gradient in SA concentration from surface to the microcapsule center). Further, while the SCS located near the droplet surface can immediately form IPEC with incoming PMCG, most of SCS is initially embedded in the forming alginate network through which it diffuses toward the surface until it meets PMCG diffusing into the microcapsule in the opposite direction, which forms the PMCG-SCS IPEC layer visualized by CRM above.[24] The residual SCS in the microcapsule core is presumably the high-MW fraction that became trapped within the quickly developing alginate matrix, unable to reach the PMCG polycation. Note that we do not consider secondary interactions (e.g., PMCG-SA or SCS-Ca^{2+}) in this simplified picture.

Considering the CRM results, the PMCG microcapsule can be viewed as an alginate microbead bolstered with two IPEC-based layers that lend the microcapsule its specific mechanical properties and visual appearance. It can be envisaged that the IPEC-based layers act as additional interfaces (semipermeable membranes) modulating the overall microcapsule permeability. This may result in a complex permeation regime where different parts of the microcapsule are characterized by different MWCO values and different affinity toward charged species, as indicated by the permeability results obtained using the labeled IgG/CLSM and iSEC methods.

Figure 4 reveals that the changes to the concentration profiles of SA, SCS, and PMCG in postmodified microcapsules were not particularly pronounced in most cases. For microcapsules postmodified with high-MW polycations (CQM, CQH, DQM), the concentration of the base polymers apparently increased in the microcapsule surface region. This is true especially for the concentration of SA in CQM- and CQH-postmodified microcapsules that almost doubled when compared to the parent microcapsule. This may be interpreted as an increase in the density of the hydrogel network in the membrane region and related to the decreased membrane

https://doi.org/10.1021/acs.biomac.4c00222
Biomacromolecules 2024, 25, 4118−4138

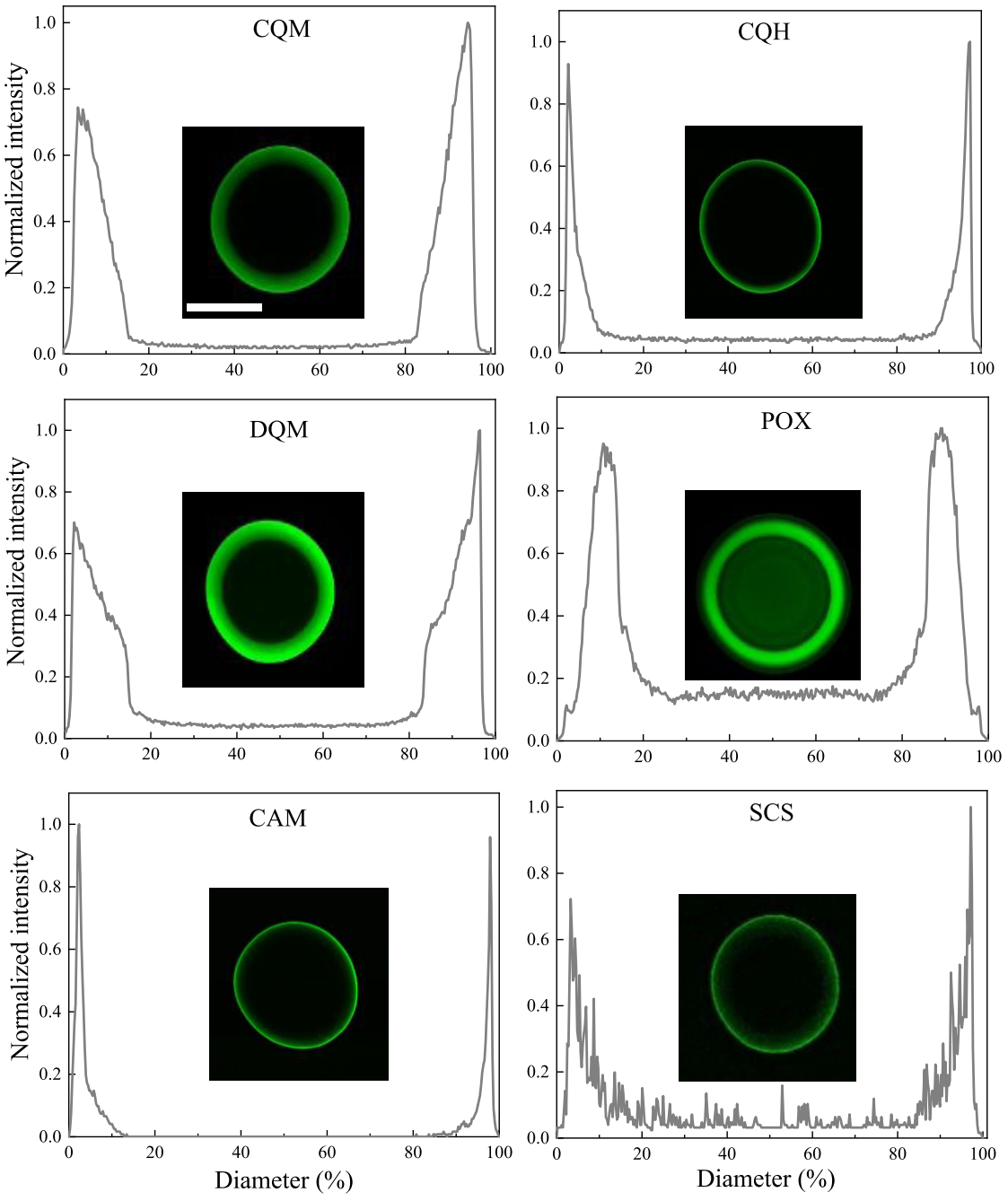

Figure 5. CLSM intensity profiles (normalized to the maximum intensity) expressing the spatial distribution of FITC-labeled PEs at the equatorial microcapsule cross-section in postmodified microcapsules ("after preparation") plotted against the diameter expressed as a percentage where edges of the microcapsule are set at 0 and 100%. The insets show the individual fluorescence microcapsule images. Bar equals to 0.5 mm.

thickness previously observed for these microcapsules (Figure 1b). The postmodification did not have a significant impact on the concentration of the base polymers in the surface region for the remaining studied microcapsules. Focusing on the PMCG and SCS global maxima (the inner IPEC layer), we can observe a similar development for CQM, CQH, DQM, and CAM-postmodified microcapsules, consisting in a minor decrease in SCS concentration (that still reaches ca. 13 wt %) and a more pronounced drop in PMCG concentration to approximately 10 wt %. In the case of POX-postmodified microcapsules, the changes were qualitatively similar, but the decrease in the SCS and, particularly, PMCG concentration was more pronounced. Remarkably, the microcapsule post-modification with SCS resulted in clear spatial redistribution of PMCG and SCS in the microcapsule volume, which is visualized as splitting of the PMCG/SCS maximum in the concentration profile (Figure 4). The fact that only SCS was found to substantially disrupt the original PMCG-SCS IPEC can be ascribed to the strong Coulombic interaction between SCS and PMCG (a guanidine-based polycation). Recent studies have shown that guanidine-based polycations, such as guanylated poly(allylamine), form exceptionally strong IPECs due to the formation of contact ion pairs between guanidinium groups, creating $^{2+}$ charges along the polycation chain.[59,60] Polycations used for microcapsule postmodification are

https://doi.org/10.1021/acs.biomac.4c00222
Biomacromolecules 2024, 25, 4118−4138

probably considerably less effective in disrupting the original strong PMCG-SCS IPEC owing to their lower charge density.

On the whole, it can be concluded that the microcapsule postmodification with PEs has an impact on the distribution of the base polymers within microcapsule volume. The extent of this impact depends on the charged group identity and charge type/density of the PE used. Surprisingly, the observed changes to the spatial distribution of base polymers do not seem to significantly influence the mechanical properties (compression resistance) of the microcapsules when studied in the "after preparation" stage (Figure 1c). This observation holds true even for the SCS-postmodified microcapsule, as this variant shows, after preparation, compression resistance basically identical to that of the parent PMCG microcapsules. Nevertheless, we presume that the base polymer spatial redistribution makes some of the microcapsules susceptible to additional structural changes when exposed to the challenging *in vivo* environment, which ultimately leads to the marked differences in mechanical properties observed for the explanted microcapsules (Figure 1c).

As it proved difficult to find characteristic Raman vibrations suitable for following the spatial distribution of all polymers used for microcapsule postmodification via CRM, we resorted to the CLSM imaging of microcapsules postmodified with FITC-labeled polymers. We validated this approach by comparing the CLSM- and CRM-based relative intensity profiles for CQM- and CQH-postmodified microcapsules, observing a good qualitative match (Figure S10). The experimental approach used to obtain the CRM data is covered in Table S6, Figure S11, and in the accompanying discussion.

Figure 5 provides the fluorescence intensity profiles obtained by the CLSM analysis of microcapsules postmodified with FITC-labeled PEs. Additionally, fluorescence images of the individual studied microcapsules are shown to facilitate their comparison. In general, three spatial distribution patterns can be observed, featuring the labeled polymers: (i) localized in a thin shell close to the microcapsule surface (CQH, CAM, SCS), (ii) distributed throughout the membrane (CQM, DQM), and (iii) penetrating the entire microcapsule volume (POX). The observed distribution patterns indicate that MW and charge jointly control the PE permeation within the parent microcapsules. This is particularly well-visible for the polycationic PEs where CQH, as the polycation of the highest MW and charge density, is found only in a thin layer close to the microcapsule surface while the less densely charged CQM penetrates deeper into the membrane. DQM, which has even lower charge density and also contains a significant low-MW fraction (Figure S2), is then able to permeate throughout the whole membrane region, with its progress further into the core probably limited by the PMCG-SCS IPEC layer that has been previously identified by CRM. Presumably, this IPEC layer plays the role of an additional inner interface characterized by a lower MWCO value than the outer interface located close to the microcapsule surface (represented by the other local base polymer concentration maxima identified by CRM).

The results from the IgG permeability assay presented above also support this hypothesis. Consequently, in the iSEC experiments discussed earlier, permeation of standards may be limited to the microcapsule region between these two interfaces, with the obtained MWCO value related exclusively to the outermost interface. Furthermore, POX contains a considerable low-MW fraction (MW $\sim 10^3$ based on the SEC data in Figure S2) that is obviously able to penetrate through the inner IPEC layer interface into the microcapsule core. We presume that the permeation and retention of (sufficiently low-MW) polycations within the whole microcapsule volume is prevalently mediated by electrostatic interactions with the omnipresent SA, with some contribution of the (unbound) residual SCS located in the microcapsule core also possible. On the other hand, the polycations do not appear to colocalize with SCS participating in the PMCG-SCS IPEC formation. This supports our former notion of the high stability of the PMCG-SCS IPEC. The low MW of PMCG probably facilitates the high degree of saturation of negative charges on SCS, making the PMCG-SCS IPEC mostly electro-neutral and "invisible" for other PEs, particularly those that are unable to disrupt the strong PMCG-SCS interactions. This may explain why some fractions of the high-MW labeled SCS seem to penetrate deeper into the microcapsule membrane when compared to the much lower-MW CAM polyanion.

Finally, it can be observed in the CLSM intensity profiles that the fluorescence signal maxima are located under the microcapsule surface (approximately at 5% of the microcapsule diameter), possibly indicating that the postmodification PEs are effectively "hidden" beneath a thin shell of hydrogel material. In some cases, this observation could be ascribed to technical limitations of the method, particularly when considering the partial misalignment of the CRM and CLSM profiles shown in Figure S10. However, in the case of POX-postmodified microcapsule (Figure 5), the negligible presence of labeled POX at the microcapsule surface is clearly visible in both the relative intensity profile and the provided fluorescence image of the microcapsule. Clearly, the actual localization of the postmodification PEs may be highly relevant with respect to the actual surface charge and, consequently, the microcapsule biocompatibility. This aspect is further discussed in the section on zeta potential analysis.

In an attempt to rationalize the aforementioned impact of the CMRL treatment on the MWCO values determined by iSEC, we briefly investigated the CMRL-treated CQM-postmodified microcapsules by CRM and CLSM. In Figure S12, the concentration profiles of the base polymers obtained by CRM are shown for CQM-modified microcapsules alongside the parent microcapsules (both treated with CMRL). Interestingly, the CMRL treatment inflicted only negligible changes to both profiles when compared to the data obtained for the "after preparation" microcapsules shown previously in Figure 4. Further, Figure S13 provides the comparison of the CLSM relative intensity profiles of CQM-postmodified microcapsules in the "after preparation" and "after CMRL treatment" phases. The differences are marginal also in this case. These findings suggest that the sharp drop in MWCO values caused by the CMRL treatment is not caused by the redistribution of polymeric components within the microcapsule volume. Instead, it can be envisaged that some of the more than 50 components of the CMRL medium (including amino acids, vitamins, inorganic salts, or glucose) trigger additional cross-linking reactions in the hydrogel network, leading to the observed decreased MWCO. As discussed above, the MWCO value is thought to be defined by the polymeric network layer located close to the microcapsule surface. We therefore assume that the additional CMRL-triggered cross-linking mainly occurs in this outer microcapsule region. On the whole, these findings highlight the complexity of processes underlying microcapsule behavior in different

https://doi.org/10.1021/acs.biomac.4c00222
Biomacromolecules 2024, 25, 4118−4138

environments and determining its potential success in the target application.

Zeta Potential Analysis. We expected that the parent microcapsule postmodification with different types of PEs could have a significant impact on the microcapsule surface charge, with possible consequences for microcapsule biocompatibility. To study this important parameter, we determined the zeta potential[61] for all the microcapsule types studied herein. Surprisingly, both the parent and postmodified microcapsules exhibited net negative charge regardless of PEs used for the postmodification (Figure 6). The zeta potential

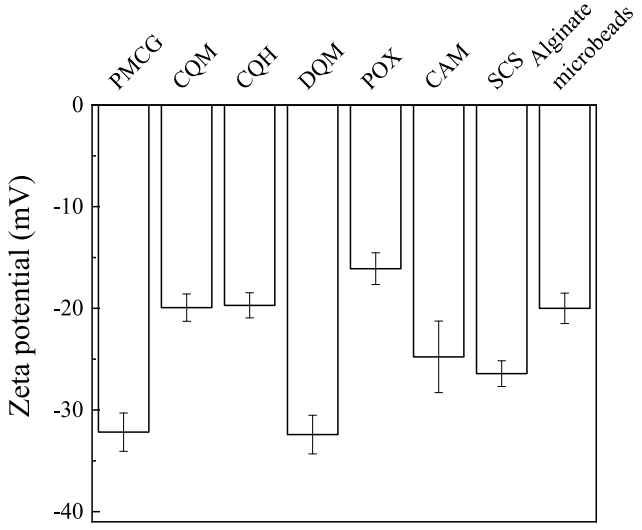

Figure 6. Zeta potential values determined in 0.1 mol·L^{-1} NaCl at pH 7.4 for parent (denoted as PMCG) and postmodified microcapsules and for alginate microbeads.

values ranged from approximately −32 mV for the parent and DQM-postmodified microcapsules to approximately −15 mV for the POX-postmodified microcapsule. It is difficult to rationalize the specific values obtained for different microcapsule types. Nevertheless, the observed negative charge of the microcapsule surface could be ascribed to SA representing the major charged polymeric component in this region, with the charges of the PMCG-SCS IPEC being largely compensated as discussed above. This assertion is supported by the apparently low presence of postmodification PEs in the outermost microcapsule layer as indicated by the CLSM data above. For comparison, we also determined zeta potential for standard alginate microbeads prepared according to Veiseh et al.,[18] with the obtained value (−20 mV) found to be close to the values measured for the studied microcapsules (Figure 6). Negative zeta potentials were previously determined also for other alginate-based microcapsules involving IPEC between alginate and chitosan[61] or poly(L-lysine).[62] However, in these studies the 0.001 mol·L^{-1} concentration of a background electrolyte was used, exposing microcapsules to hypoosmotic conditions, which may affect zeta potential values. In our work, 0.1 mol·L^{-1} NaCl was used as the background electrolyte to provide close-to-physiological ionic strength and to suppress possible artifacts stemming from hypoosmotic conditions. The finding that the postmodified PMCG microcapsules retain negative surface charge irrespective of the PE used for the postmodification could be of importance to protein absorption profiles.[63]

Human Whole Blood Assay. The impact of the postmodification with PEs on the microcapsule inflammatory and coagulation potentials was assessed by the human WBA.[29] This model is well-suited for revealing the inflammatory potential of various microsphere types and can be helpful in designing low-inflammatory microspheres for human recipients.[10] Alongside the differently postmodified PMCG microcapsules, we also evaluated alginate microbeads (Ca/Ba beads) and alginate-PLL microcapsules (AP) for comparison.[28−30] This allowed us to assess the performance of postmodified PMCG microcapsules in the context of related, but compositionally much less complex, microsphere types.

Figure 7a shows that both the parent and postmodified microcapsules increased the prothrombin fragment 1 + 2 (PFT1.2) level as compared to saline and Ca/Ba beads, which indicates an increased potential of coagulation activation for these microcapsules. Particularly, coagulation activation by SCS-postmodified microcapsules was comparable to the level of *E. coli*. The obtained results agree with the previous study by Gravastrand et al., who demonstrated that PTF1.2 was rapidly and significantly induced by PMCG microcapsules but not by Ca/Ba beads.[28] In the former study, PMCG microcapsules were found to activate the intrinsic pathway of coagulation via the activation of factor FXII. Figure 7a reveals that this effect was significantly reduced for microcapsules postmodified with CQM, CQH, POX, and CAM.

Figure 7b illustrates that the plasma concentration of soluble terminal complement complex (TCC) slightly increased in the presence of microcapsules postmodified with polycations containing quaternized amino groups (CQM, CQH, and DQM) as well as with SCS, when compared to the parent microcapsule. Moreover, the TCC levels induced by the parent microcapsules and by CAM- and POX-postmodified microcapsules were similar to Ca/Ba beads, i.e., lower than the negative control (saline). Note that TCC induction by the saline control is related to the background activation by the polypropylene tubes.[29] In previous studies, PMCG microcapsules induced TCC at lower levels when compared to AP microcapsules.[28,29] In the present study, this behavior was confirmed for the parent microcapsules as well as for microcapsules postmodified by PEs, which may be ascribed to the generally higher strength of interactions holding the participating PEs in the microcapsule as compared to the relatively weak IPEC between alginate and PLL.

Figure 7c highlights that some of the studied microcapsules increased the level of CD11b on both monocytes and granulocytes as compared to the saline control. The expression of CD11b is a sensitive marker for leukocyte activation, with common triggers being complement anaphylatoxin C5a or LPS.[64] An increase in CD11b was observed for CQM-, CQH-, DQM-, and SCS-postmodified microcapsules, reaching the level obtained for AP microcapsules. On the other hand, POX- and CAM-modified microcapsules behaved similarly to Ca/Ba beads. We have previously shown for the earlier version of PMCG microcapsules that low amounts of highly positively charged anaphylatoxins are present,[29] possibly reflecting their enhanced adsorption to the microcapsule surface. The data in Figure 7c may thus indicate the postmodification influence on the highly positively charged anaphylatoxins binding to the negatively charged microcapsule surface (Figure 6) and on the CD11b expression. Nevertheless, we cannot completely exclude the possibility that a polycation release triggered the CD11b expression directly.

https://doi.org/10.1021/acs.biomac.4c00222
Biomacromolecules 2024, 25, 4118−4138

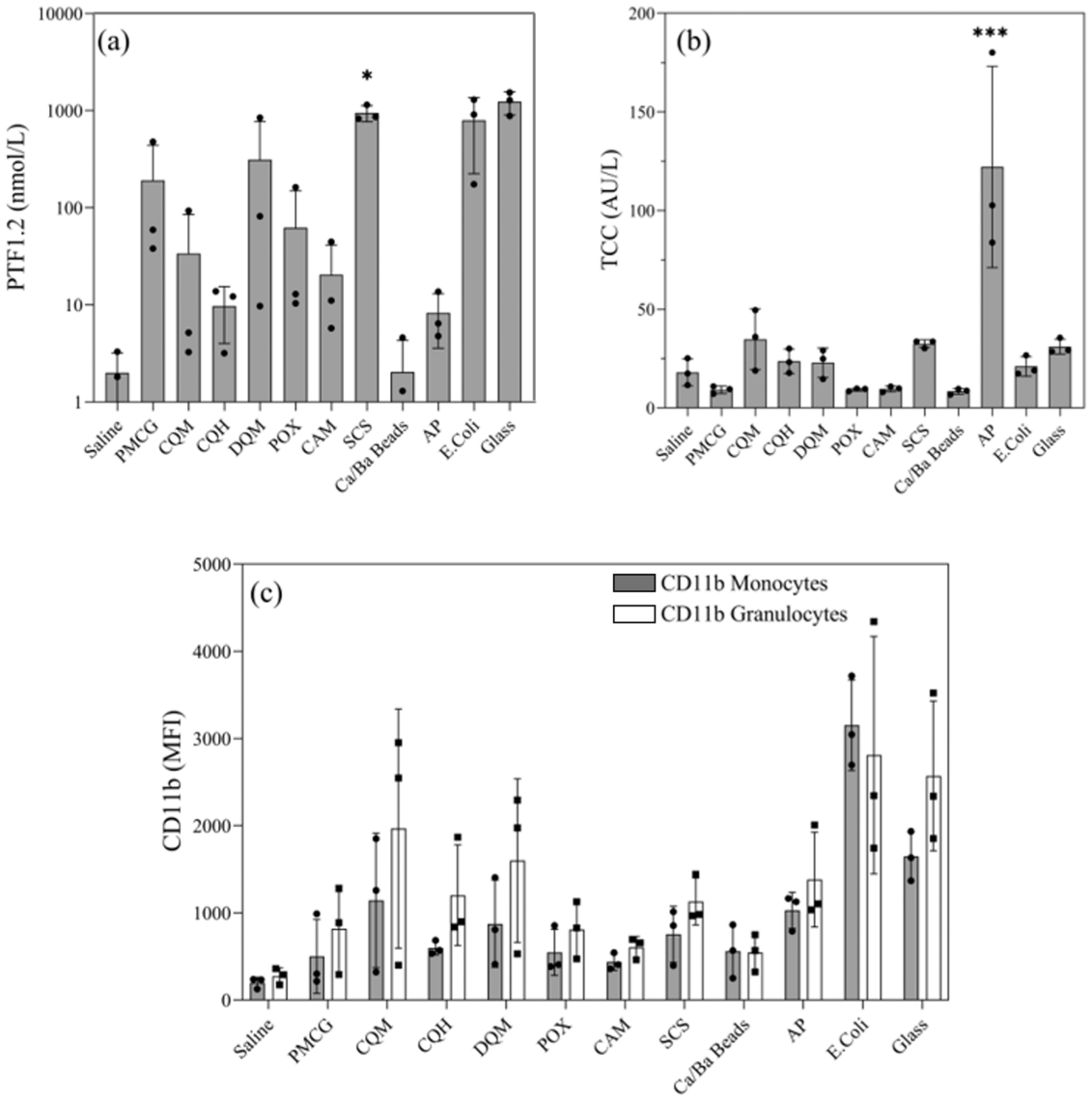

Figure 7. Inflammatory potential of microcapsules measured in a lepirudin-based human WBA (n = 3 donors, dots represent the individual measurements): (a) coagulation activation reflected by prothrombin fragment 1 + 2 (PTF1.2), (b) complement activation by plasma concentration of soluble terminal complement complex (TCC), and (c) expression of CD11b on monocytes and granulocytes given as the mean fluorescence activity (MFI) after 1 h incubation. Saline solution was used as a negative control, and *E. coli* and glass were employed as positive controls.

Figures 8 and S14 reveal that cytokine induction by both the parent and postmodified microcapsules was generally at a similar level as for the saline control. The only exception was the SCS-postmodified microcapsules that showed a comparatively higher degree of cytokine induction. CQM-postmodified microcapsules showed proinflammatory cytokines (IL-6, IL-1β, MIP-1α, and TNF-α) induction at levels comparable to AP microcapsules, i.e., slightly higher than for the parent PMCG microcapsule. Further, Figure 8 also shows comparatively increased MIP-1α concentrations for the parent as well as most of the postmodified microcapsules. MIP-1α is considered as a proinflammatory chemokine due to its role in recruiting monocytes, macrophages, neutrophils, and T-lymphocytes, initiating the production of other proinflammatory cytokines.[65,66] In addition, the parent and the postmodified microcapsules, with the exception of SCS, showed decreased induction of cytokines such as Eotaxin, PDGF-BB, IL-4, and INF-γ, as compared to saline control (Figures 8 and S14). The CQM-, DQM-, and SCS-postmodified microcapsules showed slightly elevated induction of proinflammatory cytokines (IL-6, IL-1β, MIP-1α, TNF- α, MIP-1β, MCP-1, and INF-γ), anti-inflammatory cytokines (IL-10 and IL-1Ra), growth factors (VEGF, G-CSF, GM-CSF, and FGF), and T cell activating cytokines (IL-5, IL-2, IL-4, and IL-17) compared to the remaining studied microcapsules. The chemokine IL-8 is influenced by complement activation; the production of complement factor C5a enhances IL-8 production through the MAPK signaling pathway.[67] The low IL-8 induction by microcapsules could thus reflect low complement activation.[68]

The WBA data show that the PE postmodification of the parent PMCG microcapsule resulted in only slight changes to the inflammatory properties and more pronounced changes to the coagulation patterns. Overall, these findings reflect that the microcapsule composition impacts on the initial innate immune response. It has been previously demonstrated that the activation of surface complement (C3 activation) is a key characteristic for inducing fibrosis of the AP microcapsules.[21] The surface activation of C3 in AP microcapsules has also been

https://doi.org/10.1021/acs.biomac.4c00222
Biomacromolecules 2024, 25, 4118−4138

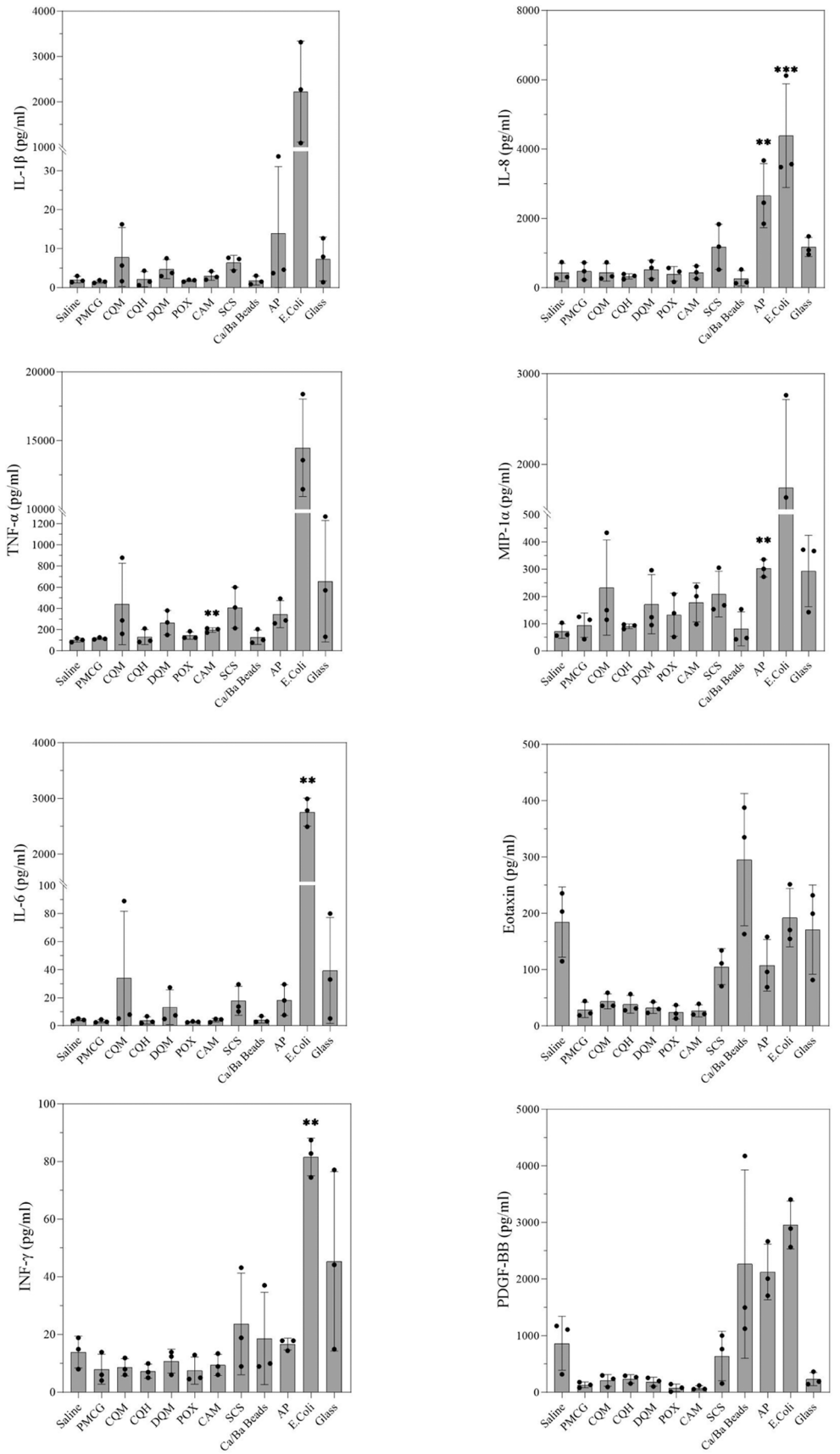

Figure 8. Effect of postmodification of PMCG microcapsules on plasma concentrations (pg/mL) of inflammatory cytokines (IL-1β, TNF-α, IL-6, and INF-y), chemokines (IL-8 (CXCL8), MIP-1α (CCL3), Eotaxin), and the growth factor PDGF-BB, following 4 h incubation in the human WBA (n = 3 donors, dots represent the individual measurements). Saline solution reflects the background activation, and *E. coli* and glass were included as positive controls.

https://doi.org/10.1021/acs.biomac.4c00222
Biomacromolecules 2024, 25, 4118−4138

shown to mediate the leukocyte adhesion through activated CD11b/CD18[69] and, thus, could be a starting point for fibrosis. While we did not determine the surface complement patterns on the current PE-modified PMCG microcapsules, we have previously shown that earlier versions of the parent PMCG microcapsules exhibited a rapid, yet modest and decreasing C3-stain,[29] which could relate to an initial activation that is inhibited further. The lower TCC induction by the PE-modified PMCG microcapsules in the current study, as compared to the AP microcapsules, could be related to a generally lower complement activation potential. Both the complement and coagulation activation patterns for other alginate-based microspheres have been recently demonstrated to depend on the complex interplay of activating and inhibitory proteins.[70] The variability in the inflammatory and coagulation-inducing patterns registered herein could thus be caused by the complexity of protein absorption patterns.

An ultimate goal of the human whole blood model is to predict the fibrotic outcome by the initial inflammatory potentials. Our data demonstrate, however, that this is not straightforward, which could be related to the complexity of the underlying (and possibly counteracting) mechanisms. While some of the PFO-inducing postmodified microcapsules (SCS) showed the highest coagulation activation (PTF1.2) and complement (TCC) of all the tested microspheres, others (CAM and POX) were among the lowest TCC inducers. Further, the CQM-postmodified microcapsules, showing great promise with regard to PFO reduction, exhibited intermediate PTF1.2 induction while being among the highest TCC inducers. In addition, this microcapsule induced the CD11b and inflammatory cytokines IL-1β, TNF, and IL-6. Since the endotoxin content was not measured, we cannot fully exclude its impact on the CQM profile. The AP microcapsules are known to induce PFO,[21] which could be related to their prominent building of the complement C3-convertase on the microcapsules surface, representing a cell-adhesion ligand through leukocytes CD11b/CD18.[69] Inhibitory studies by Ørning et al. demonstrated that the inflammatory cytokine induction potential was directly dependent on the activated C3 at the material surface and the binding of the leukocyte CD11b/CD18.[69] In contrast, in earlier studies, PMCG microcapsules promoted only minor C3 deposition causing the formation of C3-convertase at their surface;[29] therefore, the surface activation of complement is probably less relevant for PMCG microcapsules. This points to the mechanistic difference in surface activation of complement for these two microcapsule types.

Another interesting aspect, potentially connected to fibrosis, relates to the coagulation activation by FXII. FXII has the potential to activate plasminogen to plasmin, and thus FXII binding to the surface has been suggested to be involved in lowering the fibrin deposition.[21,70] We have previously demonstrated that PMCG microcapsules induce coagulation through FXII;[28] therefore, these mechanisms could be in play at the surface of PMCG microcapsules, which, however, remains to be elucidated.

Interestingly, the cytokines Eotaxin and PDGF-BB were found in low concentrations for the parent and most of the postmodified PMCG microcapsules while being elevated by the Ca/Ba beads. The chemokine Eotaxin (CCL11) and the growth factor PDGF-BB have both been linked to fibrosis,[71,72] but not to complement.[30] Since the Ca/Ba beads are inducing PFO in the C57BL/6 mouse model despite their low complement activation potential,[21] one entrance point could be their potential induction of profibrotic cytokines. Interestingly, the current study demonstrated that the SCS-postmodified microcapsules, previously found to promote the most prominent PFO, were the only studied microspheres inducing elevated Eotaxin and PDGF-BB. Overall, this study and previous studies demonstrate a complexity of responses linked to the material properties.

Viability and Proliferation of Encapsulated βTC3 Cells. In order to assess the possible influence of microcapsule postmodification with PEs on encapsulated cells, we studied the viability and proliferation of encapsulated βTC3 pancreatic mouse cells. βTC3 cells were previously shown to be a suitable model for studying the effect of encapsulation within a hydrogel environment on cell survival.[73] Figure 9 shows the viability and proliferation on days 1, 3, 7, 10, 14, and 28 postencapsulation, as quantified using the MTT colorimetric assay. The microcapsule postmodification did not have a negative impact in most cases as cells survived and proliferated equally (CAM) or better (CQM, CQH, DQM, POX) in the postmodified microcapsules when compared to the parent PMCG microcapsule, in particular, on days 3, 7, and 10 postencapsulation. In contrast, the survival of cells encapsulated in SCS-postmodified microcapsules was already significantly lower by day 1, which accounted for the low cell viability and proliferation observed at later time points. This observation indicates that the postmodification with SCS creates a cytotoxic environment for encapsulated cells. While the reasons are not immediately clear, we speculate that the additionally introduced SCS that does not get bound within an IPEC may be susceptible to the autocatalytic acidic hydrolysis of its organic sulfate ester groups, leading to the sulfuric acid release.[74] The resulting acidic environment could additionally lead to the hydrolysis of acetal linkers within the present polysaccharides (SCS, SA). Currently, we cannot completely rule out that this factor is, at least partially, responsible for the distinct properties and behavior of the SCS-postmodified

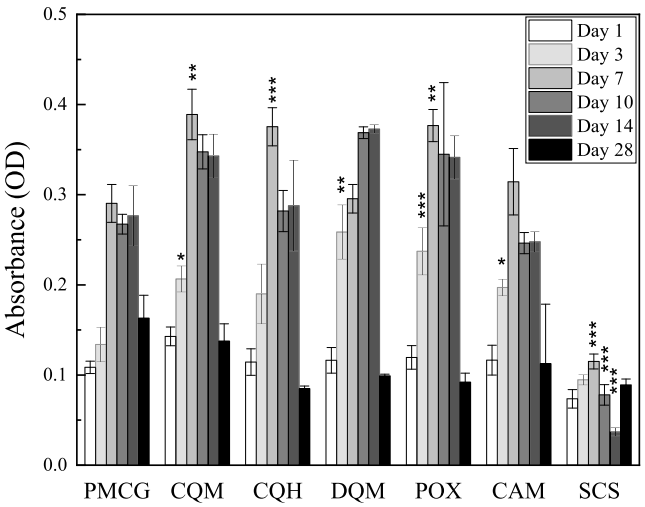

Figure 9. Viability of encapsulated βTC3 cells in the parent (denoted PMCG) and postmodified microcapsules up to 28 days postencapsulation assessed by the MTT assay. Absorbance correlates with the number of viable cells inside the microcapsules. Data points are presented as mean ± SD for three independent measurements at each time point. The statistical comparison is done between the parent and postmodified microcapsules: * $P < 0.05$, ** $P < 0.01$, *** $P < 0.001$.

https://doi.org/10.1021/acs.biomac.4c00222
Biomacromolecules 2024, 25, 4118−4138

microcapsules observed in most parts of this study. Nevertheless, Figure 9 demonstrates that the parent microcapsule and a majority of the postmodified microcapsules represent a noncytotoxic environment for encapsulated cells. This is in agreement with previous *in vivo* studies that demonstrated the survival and performance of encapsulated pancreatic islets in the PMCG microcapsules.[17,32,75,76] The decreased cell viability in all microcapsules after 14 days is presumably caused by the restricted access of cells to nutrients due to the formation of large cell aggregates as seen in Figure S15, which is typical for cells proliferating in the alginate-based microspheres.[73,77,78]

CONCLUSIONS

In conclusion, this is the first study that comprehensively evaluates the complex effects of postmodification with PEs on the properties and behavior of multicomponent alginate-based microcapsules. The postmodification was found to have a relatively limited impact on the physical properties of microcapsules when assessed immediately upon microcapsule preparation. However, this impact was significantly more pronounced for microcapsules evaluated after their retrieval from a mouse model whereby certain PEs (particularly the polycations) largely offset the generally observed drop in microcapsule compression resistance. Moreover, the postmodification showed a dramatic influence on microcapsule biocompatibility, as evaluated by the extent of PFO *in vivo*. Surprisingly, the polycation CQM-postmodified microcapsules were found to be almost free of PFO, thus manifesting better biocompatibility than the parent PMCG microcapsules. Overall, polycations provided better results than polyanions in this respect, which contrasts with some of the previous results obtained with other polycation-containing alginate-based microcapsules.

Furthermore, we conducted CRM mapping of absolute concentrations of the base PEs in the parent and postmodified microcapsules for the first time, revealing two principal PMCG-SCS IPEC layers (shells) within the microcapsule volume. The complementary CLSM mapping of the labeled postmodification PEs pointed to the important barrier function of the inner IPEC interface that restricts the access of medium- and high-MW PEs to the microcapsule core. In general, the IPEC layers proved to be resistant to disruption by most of the PEs used for postmodification; however, CRM detected that the use of SCS (a high charge density polyanion) triggered significant spatial redistribution of the IPEC polymers, which may correlate with the poor results of these microcapsules in the mechanical and biocompatibility assessments. The obtained data also suggest that the significant decrease in microcapsule permeability in complex environments (e.g., *in vivo* or in a culturing medium), detected by the IgG/CLSM and iSEC assays, is more likely caused by additional cross-linking of the hydrogel matrix rather than by the base PE redistribution.

Notably, the surface zeta potential was found to be negative for all the studied microcapsules, including those treated with polycations, with the determined values similar to that found for alginate microbeads used as a control. This indicates that the surface charge of microcapsules is mainly defined by the charge of SA that is concentrated in the surface layer, with the charges of the also present PMCG-SCS IPEC being largely mutually compensated. The postmodification PEs (particularly polycations) may then be effectively "hidden" underneath this surface layer as indicated by the CLSM mapping data.

Finally, with the exception of the polyanionic SCS, the PEs used for postmodification did not show a negative impact on the viability of model encapsulated cells, and the human WBA analysis generally revealed similar inflammatory properties and, for some of the PEs, lower coagulation potential when compared to the parent PMCG microcapsules.

On the whole, our findings highlight the complexity of processes defining the properties of alginate-based microcapsules and determining their potential success in target applications. The prepared microcapsules should not be considered as a final product but instead, as dynamic objects responding to the surrounding environment that ultimately shapes their final functional properties. Microcapsule postmodification with PEs can be both advantageous and detrimental, with even relatively small changes to the PE parameters leading to a significant impact on the final microcapsule behavior. Therefore, depending on the structure and composition of the postmodified microsphere, even the application of polycations can lead to significant enhancement of key properties. These conclusions are likely applicable to all hydrogel microspheres whose polymeric network is based on noncovalent interactions.

The main limitation of this study is the limited analytical data collected on explanted microcapsules. We believe that further advancements in techniques such as CRM will help to overcome the technical difficulties associated with the characterization of explanted microcapsules and provide essential information, e.g., on how the *in vivo* environment influences the spatial distribution of polymers within the microcapsule volume.

ASSOCIATED CONTENT

Supporting Information

The Supporting Information is available free of charge at https://pubs.acs.org/doi/10.1021/acs.biomac.4c00222.

Raman spectra, NMR spectra, and molar weight distributions of the employed polymers; additional data visualization figures; 2D PAGE analysis of the used IgG; iSEC elution and calibration curves; additional CRM and CLSM profiles; additional human WBA data; images of encapsulated βTC3 cells from the FDA/PI assay; and tables with data sets used during the CRM analysis (PDF)

AUTHOR INFORMATION

Corresponding Authors

Vladimír Raus − *Institute of Macromolecular Chemistry, Czech Academy of Sciences, 162 06 Prague 6, Czech Republic;* orcid.org/0000-0002-9424-3243; Email: raus@imc.cas.cz

Igor Lacík − *Department for Biomaterials Research, Polymer Institute of the Slovak Academy of Sciences, 845 41 Bratislava, Slovakia; National Institute of Rheumatic Diseases, 921 12 Piešťany, Slovakia;* orcid.org/0000-0001-6037-3747; Email: igor.lacik@savba.sk

Authors

Faeze Dorchei − *Department for Biomaterials Research, Polymer Institute of the Slovak Academy of Sciences, 845 41 Bratislava, Slovakia*

Abolfazl Heydari − *Department for Biomaterials Research, Polymer Institute of the Slovak Academy of Sciences, 845 41*

Bratislava, Slovakia; National Institute of Rheumatic Diseases, 921 12 Piešťany, Slovakia; orcid.org/0000-0002-7746-7480

Zuzana Kroneková − *Department for Biomaterials Research, Polymer Institute of the Slovak Academy of Sciences, 845 41 Bratislava, Slovakia; National Institute of Rheumatic Diseases, 921 12 Piešťany, Slovakia;* orcid.org/0000-0002-0265-8901

Juraj Kronek − *Department for Biomaterials Research, Polymer Institute of the Slovak Academy of Sciences, 845 41 Bratislava, Slovakia; National Institute of Rheumatic Diseases, 921 12 Piešťany, Slovakia;* orcid.org/0000-0002-0348-9740

Michal Pelach − *Department for Biomaterials Research, Polymer Institute of the Slovak Academy of Sciences, 845 41 Bratislava, Slovakia*

Zuzana Cseriová − *Department for Biomaterials Research, Polymer Institute of the Slovak Academy of Sciences, 845 41 Bratislava, Slovakia*

Dušan Chorvát − *Department of Biophotonics, International Laser Centre, Slovak Centre of Scientific and Technical Information, 841 04 Bratislava, Slovakia*

Fernando Zúñiga-Navarrete − *Department of Proteomics, Institute of Virology, Biomedical Research Center of the Slovak Academy of Sciences, 845 05 Bratislava, Slovakia*

Peter D. Rios − *CellTrans, Inc., Chicago, Illinois 60612, United States*

James McGarrigle − *CellTrans, Inc., Chicago, Illinois 60612, United States*

Sofia Ghani − *CellTrans, Inc., Chicago, Illinois 60612, United States*

Douglas Isa − *CellTrans, Inc., Chicago, Illinois 60612, United States*

Ira Joshi − *CellTrans, Inc., Chicago, Illinois 60612, United States*

Kalaiyarasi Vasuthas − *Centre of Molecular Inflammation Research (CEMIR), Department of Clinical and Molecular Medicine, Faculty of Medicine and Health Sciences, Norwegian University of Science and Technology, NO-7491 Trondheim, Norway*

Anne Mari A. Rokstad − *Centre of Molecular Inflammation Research (CEMIR), Department of Clinical and Molecular Medicine, Faculty of Medicine and Health Sciences, Norwegian University of Science and Technology, NO-7491 Trondheim, Norway*

José Oberholzer − *CellTrans, Inc., Chicago, Illinois 60612, United States; Department of Visceral Surgery and Transplantation, University Hospital Zurich, 8091 Zurich, Switzerland*

Complete contact information is available at: https://pubs.acs.org/10.1021/acs.biomac.4c00222

Notes

The authors declare no competing financial interest.

■ ACKNOWLEDGMENTS

This work was supported by the JDRF Grant No. JDRF 2-SRA-2018-521-S-B, the Chicago Diabetes Project, an international collaboration established to find a functional cure for diabetes, supported by the Washington Square Health Care Foundation, and the Slovak Research and Development Agency under contract numbers APVV-18-0480 and APVV-22-0565. This work was a part of the project "Advanced Bioactive Hydrogel Scaffolds for Regenerative Medicine" (ABSCARM), 313011BWL6 supported by the Operational Programme Integrated Infrastructure funded by the European Regional Development Fund. This work was also supported by the Ministry of Education, Youth and Sports of the Czech Republic (Grant LUAUS 23004). The authors would like to thank Eva Hipká from the Polymer Institute SAS for her assistance with the characterization of microspheres and polymers.

■ REFERENCES

(1) Zhao, L.; Skwarczynski, M.; Toth, I. Polyelectrolyte-Based Platforms for the Delivery of Peptides and Proteins. *ACS Biomater. Sci. Eng.* **2019**, *5*, 4937−4950.

(2) Stager, M. A.; Thomas, S. M.; Rotello-Kuri, N.; Payne, K. A.; Krebs, M. D. Polyelectrolyte Complex Hydrogels with Controlled Mechanics Affect Mesenchymal Stem Cell Differentiation Relevant to Growth Plate Injuries. *Macromol. Biosci.* **2022**, *22*, No. 2200126.

(3) Buriuli, M.; Verma, D. Polyelectrolyte Complexes (PECs) for Biomedical Applications. In *Advances in Biomaterials for Biomedical Applications*; Tripathi, A.; Melo, J. S., Eds.; Springer: Singapore, 2017; pp 45−93.

(4) Li, J.; Mooney, D. J. Designing Hydrogels for Controlled Drug Delivery. *Nat. Rev. Mater.* **2016**, *1*, No. 16071.

(5) Dash, M.; Chiellini, F.; Ottenbrite, R. M.; Chiellini, E. Chitosan—A Versatile Semi-synthetic Polymer in Biomedical Applications. *Prog. Polym. Sci.* **2011**, *36*, 981−1014.

(6) Kim, K.; Chen, W. C. W.; Heo, Y.; Wang, Y. Polycations and Their Biomedical Applications. *Prog. Polym. Sci.* **2016**, *60*, 18−50.

(7) Bediako, J. K.; Mouele, E. S. M.; El Ouardi, Y.; Repo, E. Saloplastics and the Polyelectrolyte Complex Continuum: Advances, Challenges and Prospects. *Chem. Eng. J.* **2023**, *462*, No. 142322.

(8) Orive, G.; Santos, E.; Pedraz, J. L.; Hernandez, R. M. Application of Cell Encapsulation for Controlled Delivery of Biological Therapeutics. *Adv. Drug. Delivery Rev.* **2014**, *67*−*68*, 3−14.

(9) Lopez-Mendez, T. B.; Santos-Vizcaino, E.; Pedraz, J. L.; Orive, G.; Hernandez, R. M. Cell Microencapsulation Technologies for Sustained Drug Delivery: Latest Advances in Efficacy And Biosafety. *J. Controlled Release* **2021**, *335*, 619−636.

(10) Rokstad, A. M. A.; Lacik, I.; de Vos, P.; Strand, B. L. Advances in Biocompatibility and Physico-Chemical Characterization of Microspheres for Cell Encapsulation. *Adv. Drug. Delivery Rev.* **2014**, *67*−*68*, 111−130.

(11) Lim, F.; Sun, A. M. Microencapsulated Islets as Bioartificial Endocrine Pancreas. *Science* **1980**, *210*, 908−910.

(12) Weir, G. C. Islet Encapsulation: Advances and Obstacles. *Diabetologia* **2013**, *56*, 1458−1461.

(13) Bochenek, M. A.; Veiseh, O.; Vegas, A. J.; McGarrigle, J. J.; Qi, M.; Marchese, E.; Omami, M.; Doloff, J. C.; Mendoza-Elias, J.; Nourmohammadzadeh, M.; Khan, A.; Yeh, C.-C.; Xing, Y.; Isa, D.; Ghani, S.; Li, J.; Landry, C.; Bader, A. R.; Olejnik, K.; Chen, M.; Hollister-Lock, J.; Wang, Y.; Greiner, D. L.; Weir, G. C.; Strand, B. L.; Rokstad, A. M. A.; Lacik, I.; Langer, R.; Anderson, D. G.; Oberholzer, J. Alginate Encapsulation as Long-Term Immune Protection of Allogeneic Pancreatic Islet Cells Transplanted into the Omental Bursa of Macaques. *Nat. Biomed. Eng.* **2018**, *2*, 810−821.

(14) Strand, B. L.; Mørch, Y. A.; Espevik, T.; Skjåk-Bræk, G. Visualization of Alginate−Poly-L-Lysine−Alginate Microcapsules by Confocal Laser Scanning Microscopy. *Biotechnol. Bioeng.* **2003**, *82*, 386−394.

(15) Orive, G.; Tam, S. K.; Pedraz, J. L.; Hallé, J.-P. Biocompatibility of Alginate−poly-l-lysine Microcapsules for Cell Therapy. *Biomaterials* **2006**, *27*, 3691−3700.

(16) Calafiore, R.; Basta, G. Alginate/Poly-L-Ornithine Microcapsules for Pancreatic Islet Cell Immunoprotection. In *Cell Encapsulation Technology and Therapeutics*; Kühtreiber, W. M.;

Lanza, R. P.; Chick, W. L., Eds.; Birkhäuser Boston: Boston, MA, 1999; pp 138−150.
(17) Wang, T.; Lacik, I.; Brissova, M.; Anilkumar, A. V.; Prokop, A.; Hunkeler, D.; Green, R.; Shahrokhi, K.; Powers, A. C. An Encapsulation System for the Immunoisolation of Pancreatic Islets. *Nat. Biotechnol.* **1997**, *15*, 358−362.
(18) Veiseh, O.; Doloff, J. C.; Ma, M.; Vegas, A. J.; Tam, H. H.; Bader, A. R.; Li, J.; Langan, E.; Wyckoff, J.; Loo, W. S.; Jhunjhunwala, S.; Chiu, A.; Siebert, S.; Tang, K.; Hollister-Lock, J.; Aresta-DaSilva, S.; Bochenek, M.; Mendoza-Elias, J.; Wang, Y.; Qi, M.; Lavin, D.; Chen, M.; Dholakia, N.; Thakrar, R.; Lacík, I.; Weir, G.; Oberholzer, J.; Greiner, D.; Langer, R.; Anderson, D. Size-and Shape-Dependent Foreign Body Immune Response to Materials Implanted in Rodents and Non-Human Primates. *Nat. Mater.* **2015**, *14*, 643−651.
(19) Vegas, A. J.; Veiseh, O.; Doloff, J. C.; Ma, M.; Tam, H. H.; Bratlie, K.; Li, J.; Bader, A. R.; Langan, E.; Olejnik, K.; Fenton, P.; Kang, J. W.; Hollister-Locke, J.; Bochenek, M. A.; Chiu, A.; Siebert, S.; Tang, K.; Jhunjhunwala, S.; Aresta-Dasilva, S.; Dholakia, N.; Thakrar, R.; Vietti, T.; Chen, M.; Cohen, J.; Siniakowicz, K.; Qi, M.; McGarrigle, J.; Graham, A. C.; Lyle, S.; Harlan, D. M.; Greiner, D. L.; Oberholzer, J.; Weir, G. C.; Langer, R.; Anderson, D. G. Combinatorial Hydrogel Library Enables Identification of Materials That Mitigate the Foreign Body Response in Primates. *Nat. Biotechnol.* **2016**, *34*, 345−352.
(20) Sremac, M.; Lei, J.; Penson, M. F. E.; Schuetz, C.; Lakey, J. R. T.; Papas, K. K.; Varde, P. S.; Hering, B.; de Vos, P.; Brauns, T.; Markmann, J.; Poznansky, M. C. Preliminary Studies of the Impact of CXCL12 on the Foreign Body Reaction to Pancreatic Islets Microencapsulated in Alginate in Nonhuman Primates. *Transplant. Direct* **2019**, *5*, No. e447.
(21) Coron, A. E.; Kjesbu, J. S.; Kjærnsmo, F.; Oberholzer, J.; Rokstad, A. M. A.; Strand, B. L. Pericapsular Fibrotic Overgrowth Mitigated in Immunocompetent Mice Through Microbead Formulations Based on Sulfated or Intermediate G Alginates. *Acta Biomater.* **2022**, *137*, 172−185.
(22) Liu, Q.; Chiu, A.; Wang, L. H.; An, D.; Zhong, M.; Smink, A. M.; de Haan, B. J.; de Vos, P.; Keane, K.; Vegge, A.; Chen, E. Y.; Song, W.; Liu, W. F.; Flanders, J.; Rescan, C.; Grunnet, L. G.; Wang, X.; Ma, M. Zwitterionically Modified Alginates Mitigate Cellular Overgrowth for Cell Encapsulation. *Nat. Commun.* **2019**, *10*, No. 5262.
(23) Demont, A.; Cole, H.; Marison, I. W. An Understanding of Potential and Limitations of Alginate/PLL Microcapsules as a Cell Retention System for Perfusion Cultures. *J. Microencapsulation* **2016**, *33*, 80−88.
(24) Kroneková, Z.; Pelach, M.; Mazancova, P.; Uhelska, L.; Trelova, D.; Razga, F.; Nemethova, V.; Szalai, S.; Chorvat, D.; McGarrigle, J. J.; Omami, M.; Isa, D.; Ghani, S.; Majkova, E.; Oberholzer, J.; Raus, V.; Siffalovic, P.; Lacik, I. Structural Changes in Alginate-Based Microspheres Exposed To In Vivo Environment as Revealed By Confocal Raman Microscopy. *Sci. Rep.* **2018**, *8*, No. 1637.
(25) Mørch, Ý. A.; Donati, I.; Strand, B. L.; Skjak-Braek, G. Effect of Ca^{2+}, Ba^{2+}, and Sr^{2+} on Alginate Microbeads. *Biomacromolecules* **2006**, *7*, 1471−1480.
(26) Lacík, I. Polymer Chemistry in Diabetes Treatment by Encapsulated Islets of Langerhans: Review to 2006. *Aust. J. Chem.* **2006**, *59*, 508−524.
(27) Vaithilingam, V.; Steinkjer, B.; Ryan, L.; Larsson, R.; Tuch, B. E.; Oberholzer, J.; Rokstad, A. M. In Vitro and In Vivo Biocompatibility Evaluation of Polyallylamine and Macromolecular Heparin Conjugates Modified Alginate Microbeads. *Sci. Rep.* **2017**, *7*, No. 11695.
(28) Gravastrand, C.; Hamad, S.; Fure, H.; Steinkjer, B.; Ryan, L.; Oberholzer, J.; Lambris, J. D.; Lacik, I.; Mollnes, T. E.; Espevik, T.; Brekke, O. L.; Rokstad, A. M. Alginate Microbeads Are Coagulation Compatible, While Alginate Microcapsules Activate Coagulation Secondary to Complement or Directly Through FXII. *Acta Biomater.* **2017**, *58*, 158−167.
(29) Rokstad, A. M.; Brekke, O. L.; Steinkjer, B.; Ryan, L.; Kollarikova, G.; Strand, B. L.; Skjak-Braek, G.; Lacik, I.; Espevik, T.; Mollnes, T. E. Alginate Microbeads Are Complement Compatible, in Contrast to Polycation Containing Microcapsules, as Revealed in A Human Whole Blood Model. *Acta Biomater.* **2011**, *7*, 2566−2578.
(30) Rokstad, A. M.; Brekke, O.-L.; Steinkjer, B.; Ryan, L.; Kollárikóvá, G.; Strand, B. L.; Skjåk-Bræk, G.; Lambris, J. D.; Lacík, I.; Mollnes, T. E.; Espevik, T. The Induction of Cytokines by Polycation Containing Microspheres by a Complement Dependent Mechanism. *Biomaterials* **2013**, *34*, 621−630.
(31) Strand, B. L.; Ryan, T. L.; In't Veld, P.; Kulseng, B.; Rokstad, A. M.; Skjak-Brek, G.; Espevik, T. Poly-L-Lysine Induces Fibrosis on Alginate Microcapsules via the Induction Of Cytokines. *Cell Transplant.* **2001**, *10*, 263−275.
(32) Lacik, I.; Brissova, M.; Anilkumar, A. V.; Powers, A. C.; Wang, T. New Capsule with Tailored Properties for the Encapsulation of Living Cells. *J. Biomed. Mater. Res.* **1998**, *39*, 52−60.
(33) Qi, M.; Lacik, I.; Kollarikova, G.; Strand, B. L.; Formo, K.; Wang, Y.; Marchese, E.; Mendoza-Elias, J. E.; Kinzer, K. P.; Gatti, F.; Paushter, D.; Patel, S.; Oberholzer, J. A Recommended Laparoscopic Procedure for Implantation of Microcapsules in the Peritoneal Cavity of Non-Human Primates. *J. Surg. Res.* **2011**, *168*, E117−E123.
(34) Papajová, E.; Bujdoš, M.; Chorvát, D.; Stach, M.; Lacík, I. Method for Preparation of Planar Alginate Hydrogels by External Gelling Using an Aerosol of Gelling Solution. *Carbohydr. Polym.* **2012**, *90*, 472−482.
(35) Heydari, A.; Dušička, E.; Mičušík, M.; Sedlák, M.; Lacík, I. Unexpected Counterion Exchange Influencing Fundamental Characteristics of Quaternary Ammonium Chitosan Salt. *Polymer* **2021**, *220*, No. 123562.
(36) Heydari, A.; Darroudi, M.; Lacik, I. Efficient N-sulfopropylation of Chitosan with 1,3-Propane Sultone in Aqueous Solutions: Neutral pH as the Key Condition. *React. Chem. Eng.* **2021**, *6*, 2146−2158.
(37) Haladjova, E.; Smolíček, M.; Ugrinova, I.; Momekova, D.; Shestakova, P.; Kroneková, Z.; Kronek, J.; Rangelov, S. DNA Delivery Systems Based on Copolymers of Poly(2-Methyl-2-Oxazoline) and Polyethyleneimine: Effect of Polyoxazoline Moieties on the Endo-Lysosomal Escape. *J. Appl. Polym. Sci.* **2020**, *137*, 49400.
(38) Schweiger, R. G. Polysaccharide Sulfates. I. Cellulose Sulfate with a High Degree of Substitution. *Carbohydr. Res.* **1972**, *21*, 219−228.
(39) Zang, Q.; Li, Z. Synthesis of a New Cationic Acrylamide-Dicyanodiamide Macromer and Its Copolymerization with Acrylamide. *Macromolecules* **1994**, *27*, 526−531.
(40) Son, Y. J.; Jang, J.-S.; Cho, Y. W.; Chung, H.; Park, R.-W.; Kwon, I. C.; Kim, I.-S.; Park, J. Y.; Seo, S. B.; Park, C. R.; Jeong, S. Y. Biodistribution and Anti-Tumor Efficacy of Doxorubicin Loaded Glycol-Chitosan Nanoaggregates by EPR Effect. *J. Controlled Release* **2003**, *91*, 135−145.
(41) Udomrati, S.; Gohtani, S. Tapioca Maltodextrin Fatty Acid Ester as a Potential Stabilizer for Tween 80-Stabilized Oil-In-Water Emulsions. *Food Hydrocolloids* **2015**, *44*, 23−31.
(42) Anilkumar, A. V.; Lacik, I.; Wang, T. G. A Novel Reactor for Making Uniform Capsules. *Biotechnol. Bioeng.* **2001**, *75*, 581−589.
(43) Lacík, I.; Stach, M.; Kasák, P.; Semak, V.; Uhelská, L.; Chovancová, A.; Reinhold, G.; Kilz, P.; Delaittre, G.; Charleux, B.; Chaduc, I.; D'Agosto, F.; Lansalot, M.; Gaborieau, M.; Castignolles, P.; Gilbert, R. G.; Szablan, Z.; Barner-Kowollik, C.; Hesse, P.; Buback, M. SEC Analysis of Poly(Acrylic Acid) and Poly(Methacrylic Acid). *Macromol. Chem. Phys.* **2015**, *216*, 23−37.
(44) Urbanová, A.; Ezenwajiaku, I. H.; Nikitin, A. N.; Sedlák, M.; Vale, H. M.; Hutchinson, R. A.; Lacík, I. PLP-SEC Investigation of the Influence of Electrostatic Interactions on the Radical Propagation Rate Coefficients of Cationic Monomers TMAEMC and MAPTAC. *Macromolecules* **2021**, *54*, 3204−3222.
(45) Briššová, M.; Petro, M.; Lacık, I.; Powers, A. C.; Wang, T. Evaluation of Microcapsule Permeability via Inverse Size Exclusion Chromatography. *Anal. Biochem.* **1996**, *242*, 104−111.

https://doi.org/10.1021/acs.biomac.4c00222
Biomacromolecules 2024, 25, 4118−4138

(46) Schenkmayerová, A.; Bučko, M.; Gemeiner, P.; Treľová, D.; Lacík, I.; Chorvát, D.; Ačai, P.; Polakovič, M.; Lipták, L.; Rebroš, M.; Rosenberg, M.; Štefuca, V.; Neděla, V.; Tihlaříková, E. Physical and Bioengineering Properties of Polyvinyl Alcohol Lens-Shaped Particles Versus Spherical Polyelectrolyte Complex Microcapsules as Immobilisation Matrices for a Whole-Cell Baeyer−Villiger Monooxygenase. *Appl. Biochem. Biotechnol.* **2014**, *174*, 1834−1849.
(47) Briššová, M.; Lacík, I.; Powers, A. C.; Anilkumar, A. V.; Wang, T. Control and Measurement of Permeability for Design of Microcapsule Cell Delivery System. *J. Biomed. Mater. Res.* **1998**, *39*, 61−70.
(48) Shalaby, T. I.; El-Refaie, W. M. Bioadhesive Chitosan-Coated Cationic Nanoliposomes With Improved Insulin Encapsulation and Prolonged Oral Hypoglycemic Effect in Diabetic Mice. *J. Pharm. Sci.* **2018**, *107*, 2136−2143.
(49) Thanos, C. G.; Calafiore, R.; Basta, G.; Bintz, B. E.; Bell, W. J.; Hudak, J.; Vasconcellos, A.; Schneider, P.; Skinner, S. J.; Geaney, M.; Tan, P.; Elliot, R. B.; Tatnell, M.; Escobar, L.; Qian, H.; Mathiowitz, E.; Emerich, D. F. Formulating the Alginate-Polyornithine Biocapsule for Prolonged Stability: Evaluation of Composition and Manufacturing Technique. *J. Biomed. Mater. Res., Part A* **2007**, *83A*, 216−224.
(50) Lunkad, R.; Murmiliuk, A.; Hebbeker, P.; Boublík, M.; Tošner, Z.; Štěpánek, M.; Košovan, P. Quantitative Prediction of Charge Regulation in Oligopeptides. *Mol. Syst. Des. Eng.* **2021**, *6*, 122−131.
(51) Van Raamsdonk, J. M.; Chang, P. L. Osmotic Pressure Test: A Simple, Quantitative Method to Assess the Mechanical Stability of Alginate Microcapsules. *J. Biomed. Mater. Res.* **2001**, *54*, 264−271.
(52) Doloff, J. C.; Veiseh, O.; Vegas, A. J.; Tam, H. H.; Farah, S.; Ma, M.; Li, J.; Bader, A.; Chiu, A.; Sadraei, A.; Aresta-Dasilva, S.; Griffin, M.; Jhunjhunwala, S.; Webber, M.; Siebert, S.; Tang, K.; Chen, M.; Langan, E.; Dholokia, N.; Thakrar, R.; Qi, M.; Oberholzer, J.; Greiner, D. L.; Langer, R.; Anderson, D. G. Colony Stimulating Factor-1 Receptor Is a Central Component of the Foreign Body Response to Biomaterial Implants in Rodents and Non-Human Primates. *Nat. Mater.* **2017**, *16*, 671−680.
(53) Baumberger, T.; Ronsin, O. Ionic Control of Crack Propagation in Biopolymer Hydrogels. *Procedia IUTAM* **2015**, *12*, 3−9.
(54) Hilborn, J.; Bjursten, L. M. A New and Evolving Paradigm for Biocompatibility. *J. Tissue Eng. Regen. Med.* **2007**, *1*, 110−119.
(55) Takacova, M.; Hlouskova, G.; Zatovicova, M.; Benej, M.; Sedlakova, O.; Kopacek, J.; Pastorek, J.; Lacik, I.; Pastorekova, S. Encapsulation of Anti-carbonic Anhydrase IX Antibody in Hydrogel Microspheres for Tumor Targeting. *J. Enzyme Inhib. Med. Chem.* **2016**, *31*, 110−118.
(56) Adrian, E.; Treľová, D.; Filová, E.; Kumorek, M.; Lobaz, V.; Poreba, R.; Janoušková, O.; Pop-Georgievski, O.; Lacík, I.; Kubies, D. Complexation of CXCL12, FGF-2 and VEGF with Heparin Modulates the Protein Release from Alginate Microbeads. *Int. J. Mol. Sci.* **2021**, *22*, 11666.
(57) Gu, F.; Amsden, B.; Neufeld, R. Sustained Delivery of Vascular Endothelial Growth Factor with Alginate Beads. *J. Controlled Release* **2004**, *96*, 463−472.
(58) Qi, M.; Morch, Y.; Lacik, I.; Formo, K.; Marchese, E.; Wang, Y.; Danielson, K. K.; Kinzer, K.; Wang, S.; Barbaro, B.; Kollarikova, G.; Chorvat, D., Jr.; Hunkeler, D.; Skjak-Braek, G.; Oberholzer, J.; Strand, B. L. Survival of Human Islets in Microbeads Containing High Guluronic Acid Alginate Crosslinked with Ca^{2+} and Ba^{2+}. *Xenotransplantation* **2012**, *19*, 355−364.
(59) Sadman, K.; Wang, Q.; Shull, K. R. Guanidinium Can Break and Form Strongly Associating Ion Complexes. *ACS Macro Lett.* **2019**, *8*, 117−122.
(60) Kim, S.; Lee, M.; Lee, W. B.; Choi, S.-H. Ionic-Group Dependence of Polyelectrolyte Coacervate Phase Behavior. *Macromolecules* **2021**, *54*, 7572−7581.
(61) Xie, H. G.; Li, X. X.; Lv, G. J.; Xie, W. Y.; Zhu, J.; Luxbacher, T.; Ma, R.; Ma, X. J. Effect of Surface Wettability and Charge on Protein Adsorption onto Implantable Alginate-Chitosan-Alginate Microcapsule Surfaces. *J. Biomed. Mater. Res., Part A* **2010**, *92A*, 1357−1365.
(62) de Vos, P.; de Haan, B. J.; Kamps, J. A.; Faas, M. M.; Kitano, T. Zeta-potentials of Alginate-PLL Capsules: A Predictive Measure for Biocompatibility? *J. Biomed. Mater. Res., Part A* **2007**, *80A*, 813−819.
(63) Vogler, E. A. Protein Adsorption in Three Dimensions. *Biomaterials* **2012**, *33*, 1201−1237.
(64) Brekke, O. L.; Christiansen, D.; Fure, H.; Fung, M.; Mollnes, T. E. The Role of Complement C3 Opsonization, C5a Receptor, and CD14 in *E. Coli*-Induced Up-Regulation of Granulocyte and Monocyte CD11b/CD18 (CR3), Phagocytosis, and Oxidative Burst in Human Whole Blood. *J. Leukocyte Biol.* **2007**, *81*, 1404−1413.
(65) Deshmane, S. L.; Kremlev, S.; Amini, S.; Sawaya, B. E. Monocyte Chemoattractant Protein-1 (MCP-1): An Overview. *J. Interferon Cytokine Res.* **2009**, *29*, 313−326.
(66) Maurer, M.; Von Stebut, E. Macrophage Inflammatory Protein-1. *Int. J. Biochem. Cell Biol.* **2004**, *36*, 1882−1886.
(67) Wang, L.; Han, G.; Wang, R.; Chen, G.; Xu, R.; Xiao, H.; Li, X.; Geng, S.; Li, Y.; Li, X.; Wang, J.; Feng, J.; Riedemann, N. C.; Guo, R.; Shen, B.; Li, Y. Regulation of IL-8 Production by Complement-Activated Product, C5a, In Vitro and In Vivo During Sepsis. *Clin. Immunol.* **2010**, *137*, 157−165.
(68) Samstad, E. O.; Niyonzima, N.; Nymo, S.; Aune, M. H.; Ryan, L.; Bakke, S. S.; Lappegård, K. T.; Brekke, O.-L.; Lambris, J. D.; Damås, J. K.; Latz, E.; Mollnes, T. E.; Espevik, T. Cholesterol Crystals Induce Complement-Dependent Inflammasome Activation and Cytokine Release. *J. Immunol.* **2014**, *192*, 2837−2845.
(69) Ørning, P.; Hoem, K. S.; Coron, A. E.; Skjåk-Bræk, G.; Mollnes, T. E.; Brekke, O.-L.; Espevik, T.; Rokstad, A. M. Alginate Microsphere Compositions Dictate Different Mechanisms of Complement Activation with Consequences for Cytokine Release and Leukocyte Activation. *J. Controlled Release* **2016**, *229*, 58−69.
(70) Coron, A. E.; Fonseca, D. M.; Sharma, A.; Slupphaug, G.; Strand, B. L.; Rokstad, A. M. A. MS-Proteomics Provides Insight into the Host Responses towards Alginate Microspheres. *Materials Today Bio* **2022**, *17*, No. 100490.
(71) Bonner, J. C. Regulation of PDGF and Its Receptors in Fibrotic Diseases. *Cytokine Growth Factor Rev.* **2004**, *15*, 255−273.
(72) Jacobs, I.; Ceulemans, M.; Wauters, L.; Breynaert, C.; Vermeire, S.; Verstockt, B.; Vanuytsel, T. Role of Eosinophils in Intestinal Inflammation and Fibrosis in Inflammatory Bowel Disease: An Overlooked Villain? *Front. Immunol.* **2021**, *12*, No. 754413.
(73) Hoesli, C. A.; Kiang, R. L.; Mocinecova, D.; Speck, M.; Moskova, D. J.; Donald-Hague, C.; Lacik, I.; Kieffer, T. J.; Piret, J. M. Reversal of Diabetes by betaTC3 Cells Encapsulated in Alginate Beads Generated by Emulsion and Internal Gelation. *J. Biomed. Mater. Res., Part B* **2012**, *100*, 1017−1028.
(74) Kučerová, M.; Pašteka, M. Sulfation of Cross-linked Polysaccharides by the N,N-Dimethylformamide-SO3 Complex. *Chem. Pap.* **1975**, *29*, 697−702.
(75) Qi, M.; McGarrigle, J.; Wang, Y.; Marchese, E.; Bochenek, M.; Vaca, P.; Davis, M.; Ahn, S.; Schwartz, A.; Strand, B.; Lacík, I.; Oberholzer, J. Transplantation of Pancreatic Islets Immobilized in Alginate-Based Microcapsules: From Animal Studies to Clinical Trials. *Micro Nanosyst.* **2013**, *5*, 186−193.
(76) Wang, T.; Adcock, J.; Kühtreiber, W.; Qiang, D.; Salleng, K. J.; Trenary, I.; Williams, P. Successful Allotransplantation of Encapsulated Islets in Pancreatectomized Canines for Diabetic Management without the Use of Immunosuppression. *Transplantation* **2008**, *85*, 331−337.
(77) Bhujbal, S. V.; de Haan, B.; Niclou, S. P.; de Vos, P. A Novel Multilayer Immunoisolating Encapsulation System Overcoming Protrusion of Cells. *Sci. Rep.* **2014**, *4*, No. 6856.
(78) Hoesli, C. A.; Raghuram, K.; Kiang, R. L.; Mocinecova, D.; Hu, X.; Johnson, J. D.; Lacik, I.; Kieffer, T. J.; Piret, J. M. Pancreatic Cell Immobilization in Alginate Beads Produced by Emulsion and Internal Gelation. *Biotechnol. Bioeng.* **2011**, *108*, 424−434.

https://doi.org/10.1021/acs.biomac.4c00222
Biomacromolecules 2024, 25, 4118−4138